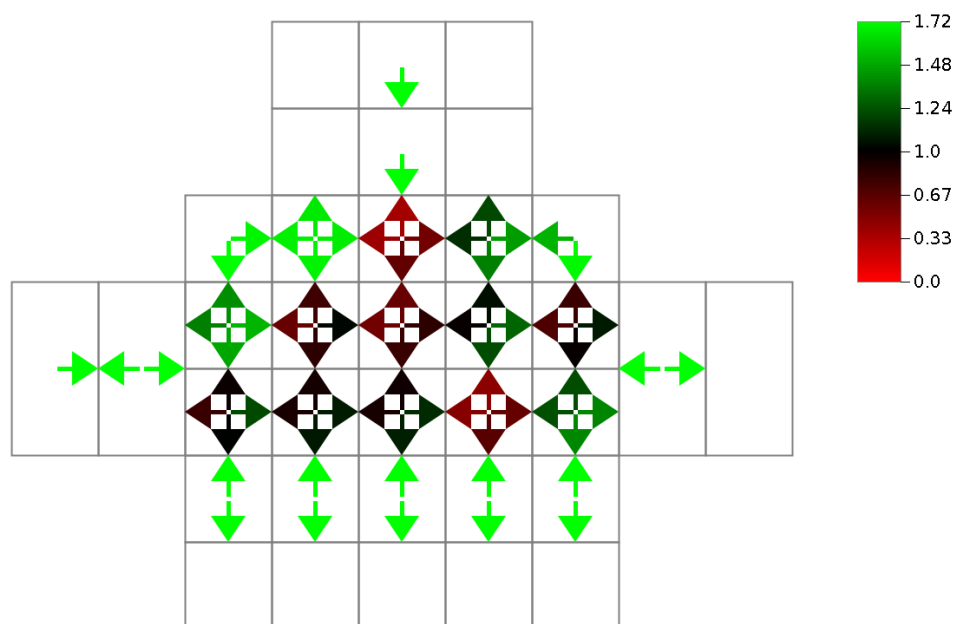


A macroscopic loading model for dynamic, anisotropic and congested pedestrian flows.

Implementation, calibration and case study analysis

Gael Lederrey



Abstract

Pedestrian facilities are more and more congested. It is important to understand the modeling of pedestrian flows to assure safety and comfort. Many models have already been developed such as the social force model and PedCTM. The problem is that either they allow for population heterogeneity or they are fast. The goal of this project is to implement a new model that has both of these characteristics.

The new model presented here is fast due to the use of a fundamental diagram. The anisotropy of this model comes from a new formulation of a fundamental diagram based on the literature, SbFD. This project gives a summary of the model and presents the new fundamental diagram. It also compares this fundamental diagram to the state-of-the-practice, Weidmann (1992). The different parameters of the model and the fundamental diagrams are calibrated using the *simulated annealing* algorithm. Finally, a case study analysis on two sets of experimental data is done to compare the performance of the fundamental diagrams.

Contents

1	Introduction	1
2	Model Framework	1
2.1	Summary of the model	1
2.2	Fundamental diagrams–density–speed relation	3
2.2.1	Weidmann	3
2.2.2	SbFD	4
2.2.3	Drake	4
2.2.4	Shape of the fundamental diagrams	4
3	Calibration	6
3.1	Parameter calibration	6
3.2	Objective function	7
3.3	Combinatorial cross-validation	7
4	Data	8
4.1	HKU – Counter-flow experiments	8
4.2	Berlin – “Science Night” experiments	10
5	Results	12
5.1	HKU – Counter-flow experiments	12
5.2	Berlin – “Science Night” controlled experiments	25
5.3	Berlin – “Science Night” ‘uncontrolled’ experiment	26
6	Discussion	27
7	Conclusion	28
	Bibliography	29
	Appendix	29
	Histograms of experiments by Wong et al. (2010) experiments	30
	Histograms of experiments by Plaue et al. (2011) experiments	32
	Boxplots of the parameters	33

1 Introduction

The study of pedestrian flows is gaining importance due to phenomena such as congestion in transportation hubs and urban facilities. It is desirable to have fast predictive models to optimize the design and operation of pedestrian environments in terms of safety, comfort and performance. So far, mostly models have been developed that have either population heterogeneity (social force model), or are fast (cellular automata), but usually not both. To consider complex networks, or for accessory problems such as demand estimation, we however need models that combine both properties.

To that end, the use of a cell transmission model for describing pedestrian flows is a promising approach. The cell transmission model is fast and can be easily calibrated thanks to its use of a fundamental diagram. For mildly congested situations, or for situations involving uni-directional flows, such a model has been successfully developed (PedCTM) (Hänseler et al.; 2014).

For problems that are both congested and multi-directional, flows are typically anisotropic, i.e., the walking speed depends on the direction. For instance for bi-directional flows on cross-walks or in shopping malls in Hong Kong, it has been shown by Lam et al. (2002) that the speed in the direction of major flow is significantly higher than in the opposite direction. Existing cell transmission models, such as the aforementioned PedCTM, cannot realistically reproduce such anisotropic phenomena.

To address this issue, we would like to develop a model that features the efficiency of the cell-transmission model, but which can additionally reproduce anisotropic flow behavior at the aggregate level, as they appear in mildly or highly congested situations for multi-directional flow patterns. Our approach lies in the use of a link-transmission model.

2 Model Framework

2.1 Summary of the model

We give here a summary of the model framework provided by Hänseler et al. (2015). All the details are given in Hänseler et al. (2015, section 3).

We consider a discrete-time discrete-space model, where each time interval $\tau \in \mathcal{T}$ is of uniform length $\Delta T > 0$. The pedestrian walking network is represented by a directed graph $\mathcal{G} = \{\Lambda, \mathcal{N}\}$ where Λ is the set of directed streams $\lambda \in \Lambda$ and \mathcal{N} the set of nodes $\nu \in \mathcal{N}$. The length of each stream is given by $L_\lambda > 0$ and the minimum length is given by $L_{\min} = \min_{\lambda \in \Lambda} L_\lambda$.

Pedestrians move along streams. Multi-directional flow is decomposed into the set of uni-directional streams. Each stream λ is associated with an area ξ , defining a space in which local streams interact. The surface size of an area ξ is denoted by $\mathcal{A}_\xi > 0$. There is no a priori assumption regarding the size and shape of an area. The set of all areas is denoted by \mathcal{X} , and the set of links associated with area ξ by Λ_ξ , with $\Lambda_\xi \subset \Lambda$ and $\Lambda_\xi \cap \Lambda_{\xi'} = \emptyset$ if $\xi \neq \xi'$.

Fig. 1 illustrates the proposed space representation at the example of a longitudinal corridor and a triangular space discretization. However, any other discretization – irregular, with varying link lengths and even disconnected areas – can in principle be envisaged.

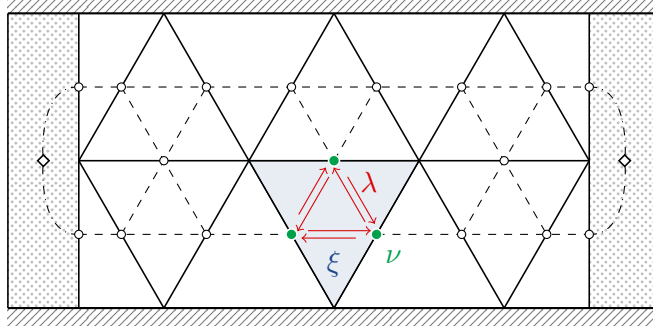


Figure 1: Illustration of space representation at the example of a longitudinal corridor. In this example, walkable space is represented by a regular network of streams $\lambda \in \Lambda$ that decompose multi-directional flow in a set of uni-directional streams that interact within areas $\xi \in \mathcal{X}$ (one is shaded in light blue). Centroids at both ends of the corridor are discernible by their star shape.

The choice of ΔT is given by the Courant-Friedrichs-Lewy (CFL) condition (Courant et al.; 1967). It can be expressed as

$$\Delta T \leq \frac{L_\lambda}{V_f}, \forall \lambda \in \Lambda \quad \implies \quad \Delta T = \frac{L_{min}}{V_f} \quad (1)$$

where V_f represents the ‘global’ free-flow speed, a calibration parameter of the model. The left part of equation 1 represents an upper bound for the time step given by the CFL condition. Since, the choice of the time discretization is not critical for the stability of this model and we don’t use it as a calibration parameter, the upper bound is used to specify it. Each link is then associated with a speed $V_{\lambda,\tau}$ that is characteristic for the stream it carries during time interval τ . This speed is calculated with a fundamental diagram that links the speed to the density k on a link λ . The concept of a fundamental diagram is given in the section 2.2.

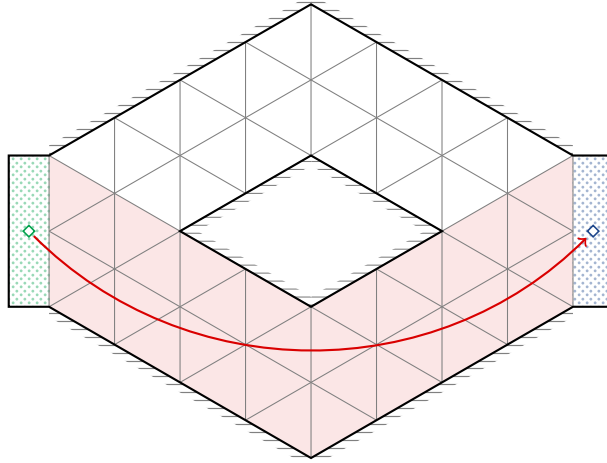


Figure 2: Illustration of the concept of route. In this example, the route is represented by the red arrow that goes from the origin node ν_o^ρ (in green) to the destination node ν_d^ρ (in blue). The accessible network \mathcal{X}_ρ for the chosen route is in light red.

A route ρ is defined as a set of links Λ_ρ and a pair of origin and destination nodes (centroids) (ν_o^ρ, ν_d^ρ) , with $\nu_o^\rho, \nu_d^\rho \in \mathcal{C} \subset \mathcal{N}$ where \mathcal{C} is the set of centroids. The set of all routes is denoted by \mathcal{R} . All the links $\lambda \in \Lambda_\rho$ are contained in an accessible network $\mathcal{X}_\rho \subset \mathcal{X}$. Generally, the route is

defined by the two centroids and the accessible network. There is no a priori restriction on the routes as they connect a pair of centroids and use a valid set of links and areas. Fig. 2 illustrates the choice of routes in the case of a network with two different paths that goes from an origin node to a destination node. The choice of the route has been done arbitrarily, the upper path can also be chosen.

Pedestrian are organized in packets. A pedestrian packet ℓ is characterized by a route ρ_ℓ , a departure time interval τ_ℓ and the number of people m_ℓ it contains. The set of all packets is denoted by $\mathcal{L} \subset \mathcal{R} \times \mathcal{T}$. The route ρ_ℓ , the departure time interval τ_ℓ and the size m_ℓ of each packet $\ell \in \mathcal{L}$ are assumed to be known a priori, and the corresponding demand matrix is denoted by $\mathcal{D} = [\rho_\ell, \tau_\ell, m_\ell] \quad \forall \ell \in \mathcal{L}$

The state of the model at any time interval is fully described by the packet-specific distribution of pedestrians on the network. The number of pedestrians associated with group ℓ on link λ during time interval τ is denoted by $\mathcal{M}_{\lambda,\tau}^\ell$ and referred to as the corresponding ‘fragment size’. The sum of all fragments on a link λ during time interval τ is denoted by $\mathcal{M}_{\lambda,\tau}$ and referred to as link accumulation. The vector of link accumulations associated with area ξ and time interval τ is denoted by $\mathcal{M}_{\xi,\tau} = [\mathcal{M}_{\lambda,\tau}]$, with $\lambda \in \Lambda_\xi$.

The ‘fragment size’ is updated using a continuity equation given by:

$$\begin{aligned} M_{\lambda,\tau+1}^\ell &= M_{\lambda,\tau}^\ell + \text{Pedestrians in packet } \ell \text{ entering link } \lambda \\ &\quad - \text{Pedestrians in packet } \ell \text{ leaving link } \lambda \\ &\quad + \text{source/sink term} \end{aligned} \tag{2}$$

The source/sink terms are used only if the link λ is adjacent to a centroid $\nu \in \mathcal{C}$.

2.2 Fundamental diagrams–density-speed relation

We give here a summary of the fundamental diagrams provided by Hänseler et al. (2015). All the details are given in Hänseler et al. (2015, section 4.1).

2.2.1 Weidmann

The fundamental diagram of Weidmann (1992) is given by:

$$V_\lambda = V_f \left\{ 1 - \exp \left[-\gamma \left(\frac{\mathcal{A}_\xi}{\mathcal{M}_\xi} - \frac{1}{k_{\text{jam}}} \right) \right] \right\} \tag{3}$$

with k_{jam} the jam density, γ a shape parameter and V_f the free-flow speed. Therefore, this fundamental diagram has three different calibration parameters. One of the particularities of this fundamental diagram is that it has a jam density. One more condition stands:

$$0 \leq \frac{\mathcal{M}_\xi}{\mathcal{A}_\xi} \leq k_{\text{jam}}$$

According to Weidmann (1992), the free-flow speed is estimated at $V_f = 1.34$ m/s, the shape parameter at $\gamma = 1.913$ m⁻², and the jam density at $k_{\text{jam}} = 5.4$ m⁻².

The only problem of this fundamental diagram is that it is isotropic. However, since it is the state-of-the-practice, it is used as the benchmark for the comparison between the different fundamental diagrams.

2.2.2 SbFD

The SbFD (Stream-based Fundamental Diagram) is inspired by [Wong et al. \(2010\)](#) and [Xie and Wong \(2014\)](#). But, these two fundamental diagrams show some problems. First, the fundamental diagram of [Wong et al. \(2010\)](#) is for bi-directional flows only. On the other hand, the fundamental diagram of [Xie and Wong \(2014\)](#) is not self-consistent. Indeed, splitting up a group into two identical groups of half the magnitude yields a different flow field. It does not guarantee a unique solution, which is inconsistent with the definition of this fundamental diagram. Therefore, we present here the simplest possible fundamental diagram inspired by the literature to illustrate the model: SbFD.

$$V_\lambda = V_f \exp\left(-\vartheta \left(\frac{\mathcal{M}_\xi}{\mathcal{A}_\xi}\right)^2\right) \prod_{\lambda' \in \Lambda_\xi} \exp\left(-\beta (1 - \cos \phi_{\lambda, \lambda'}) \frac{\mathcal{M}_{\lambda'}}{\mathcal{A}_\xi}\right) \quad (4)$$

where ϑ and β are model parameters, $\phi_{\lambda, \lambda'}$ denotes the intersection angle between two groups λ and λ' with $\phi_{\lambda, \lambda'} = 0$ if $\lambda = \lambda'$, and V_f the free-flow speed.

Eq. 4 has two distinct terms. The first exponential represents the isotropic reduction in speed due to the accumulation on the whole area \mathcal{M}_ξ . The second term, *i.e.* the product of exponentials, represents the anisotropic reduction due to the ‘friction’ with other groups, depending on their density $\mathcal{M}_{\lambda'}/\mathcal{A}_\xi$ and the intersection angle $\phi_{\lambda, \lambda'}$.

This fundamental diagram is self-consistent and guarantees a unique solution. It is also anisotropic due to the ‘friction’ and it is multi-directional due to the intersection angle $\phi_{\lambda, \lambda'}$.

2.2.3 Drake

The fundamental diagram of [Drake et al. \(1967\)](#) is the isotropic version of SbFD. Indeed, if the model parameter β is set to 0, then we have:

$$V_\lambda = V_f \exp\left(-\vartheta \left(\frac{\mathcal{M}_\xi}{\mathcal{A}_\xi}\right)^2\right) \quad (5)$$

with ϑ a model parameter, and V_f the free-flow speed.

This fundamental diagram does not have the property of anisotropy and is also uni-directional. Therefore, it is used to show the improvement the anisotropic part of SbFD can bring.

2.2.4 Shape of the fundamental diagrams

Fig. 3 shows the three fundamental diagrams presented before. Weidmann and Drake’s fundamental diagrams are presented with a uni-directional flow, since they are uni-directional. However, SbFD is presented with the whole range of all possible flow compositions. The area covers all possible speeds. The two bounds are given by two particular cases of counter flow, once where a pedestrian walks with everyone else, and once where a pedestrian walks against everyone. \mathcal{M}_λ denotes the accumulation of the major flow and $\mathcal{M}_{\lambda'}$ the accumulation of the minor flow. Therefore, SbFD is given by:

$$\frac{V_\lambda}{V_f} = \exp\left(-\vartheta \left(\frac{\mathcal{M}_\lambda + \mathcal{M}_{\lambda'}}{\mathcal{A}_\xi}\right)^2\right) \exp\left(-\beta (1 - \cos \phi_{\lambda, \lambda'}) \frac{\mathcal{M}_{\lambda'}}{\mathcal{A}_\xi}\right)$$

where $\cos \phi_{\lambda, \lambda'} = -1$ because the two flows are counter-flows. The upper bound, the black solid line, is the relation found when the minor flow is zero, *i.e.* $\mathcal{M}_{\lambda'} = 0$. Therefore, the upper bound for SbFD becomes:

$$\frac{V_{\lambda}}{V_f} = \exp(-\vartheta k^2)$$

where $k = \mathcal{M}_{\lambda}/\mathcal{A}_{\xi}$ is the density. This expression of SbFD is the same as the expression of Drake's fundamental diagram with ϑ the model parameter given by the calibration on SbFD (different from the one calibrated with Drake's fundamental diagram).

The lower bound, the black dashed line, is found when the major flow is zero, *i.e.* $\mathcal{M}_{\lambda} = 0$. Therefore, the lower bound for SbFD becomes:

$$\frac{V_{\lambda}}{V_f} = \exp(-\vartheta k^2) \exp(-2\beta k)$$

where $k = \mathcal{M}_{\lambda'}/\mathcal{A}_{\xi}$ is the density.

Therefore, depending on the ratio of the flows, SbFD can take any values between the lower and the upper bound.

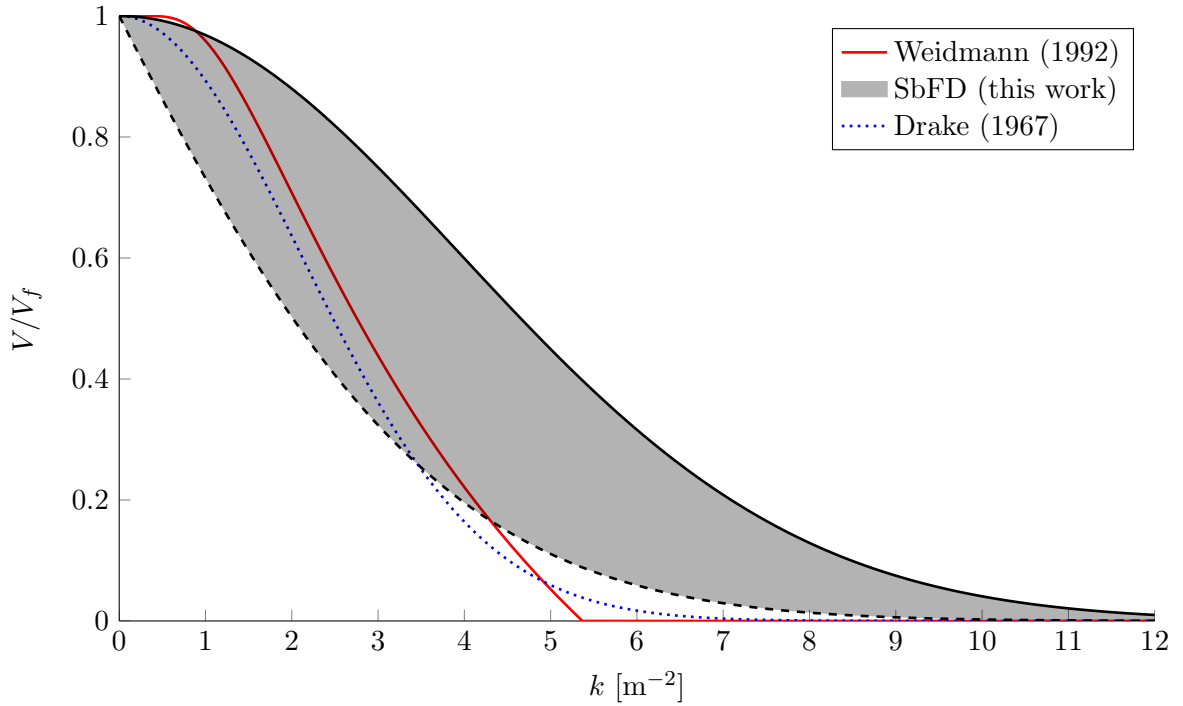


Figure 3: Illustration of the three fundamental diagrams presented before: Weidmann, SbFD, and Drake. The parameters used to illustrate the fundamental diagrams are the ones found by the full-set calibration, see section 5.1.

Fig.4 illustrates the SbFD in two dimensions: the total density and the density ratio. The upper bound of figure 3 corresponds to the value of 1 in the density ratio and the lower bounds to the value of 0 in the density ratio.

This figure already gives an idea of the benefits of an anisotropic fundamental diagram. Indeed, we see on figure 4 that if the total density is high and if the density ratio is asymmetric, then the normalized speed of the two flows will be different.

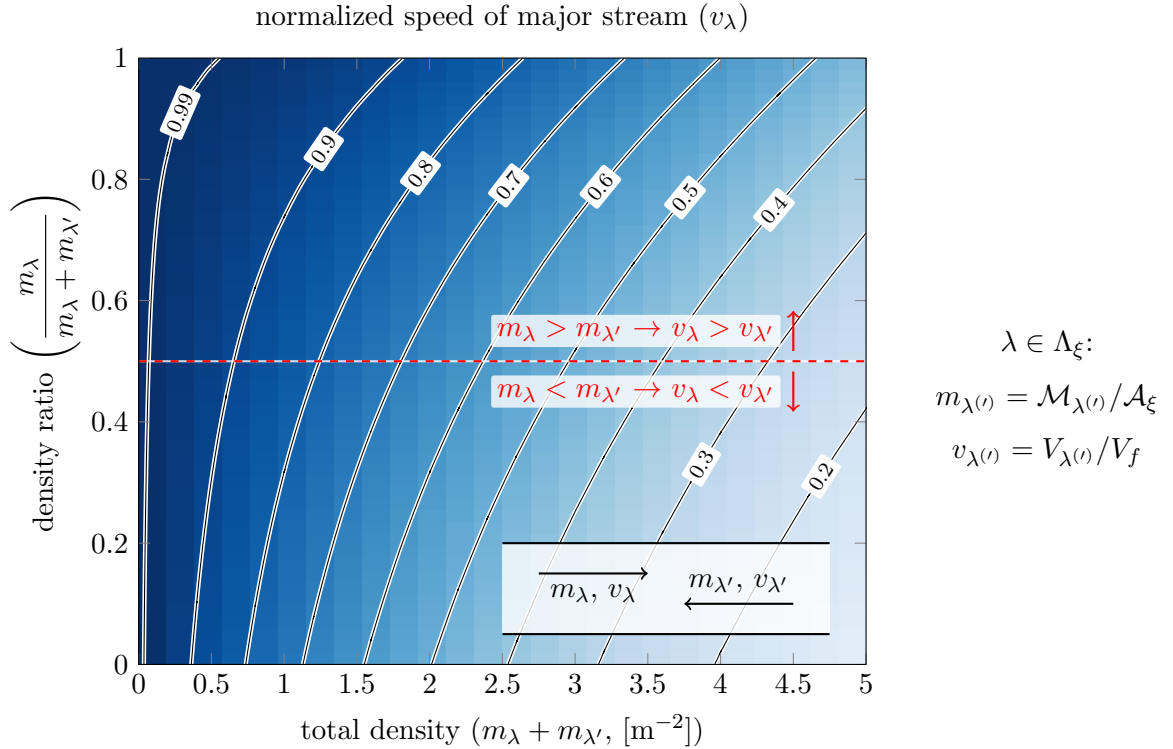


Figure 4: Illustration of SbFD in two dimensions. The parameters used to illustrate the fundamental diagrams are the ones found by the full-set calibration, see section 5.1.

3 Calibration

3.1 Parameter calibration

Let \mathbf{z} denote the set of random variables representing the parameters of the current fundamental diagram. \mathbf{z} is equal to:

- (V_f, γ, k_f, μ) for Weidmann
- $(V_f, \vartheta, \beta, \mu)$ for SbFD
- (V_f, ϑ, μ) for Drake

μ is the weight of the logit-type model of the en-route path choice model. It is not discussed in this paper, see Hänseler et al. (2015). The other parameters are defined in section 2.2.

We assume that these parameters are random variables and uncorrelated. In order to find the optimum value \mathbf{z}^* , we use a simulation-based technique called *Simulated Annealing*. Indeed, the space of parameters can be vast, therefore using a simulation-based technique gives a good approximation of the global optimum.

For each parameter, we give a lower and an upper bound. We can then define the set of feasible

parameters \mathcal{P} , a space of n dimension where n is the number of parameters to calibrate. Let $V(\mathbf{z})$ be a non-negative function defined on $\mathbf{z} \in \mathcal{P}$. We are interested in finding the minimal value of $V(\mathbf{z})$, *i.e.*

$$\mathbf{z}^* = \arg \min_{\mathbf{z}} V(\mathbf{z}) \quad (6)$$

At the beginning of the calibration, an initial vector of valid parameters $\mathbf{z}_0 \in \mathcal{P}$ is given. Then, the parameter will be randomly changed with a maximum step size. Further details of simulated annealing are given in [Farooq et al. \(2013\)](#).

3.2 Objective function

The idea of calibrating the model and the fundamental diagrams is to find the vector \mathbf{z} such that the output of the model is as close as possible to some observed data. The calibration is based on travel times of pedestrian packets. The objective function is defined by a *weighted squared error on travel times*. The idea of using different weights¹ for each packet is to equalize the effect of each group on the objective function. The weights are given by:

$$w_\ell = \frac{m_\ell}{\sum_{\ell' \in \mathcal{L}} m_{\ell'} \cdot \mathcal{I}_{\ell, \ell' \in \mathcal{K}}}$$

where \mathcal{I} is the indicator function and $\{\ell, \ell' \in \mathcal{K}\}$ means that packets ℓ and ℓ' are associated with same group. Therefore, the objective function is given by:

$$V_{\text{calib}}(\mathbf{z}) = \sum_{\ell \in \mathcal{L}(\mathbf{z})} w_\ell \left(\overline{TT}_\ell^{\text{sim}} - \overline{TT}_\ell^{\text{obs}} \right)^2 \quad (7)$$

3.3 Combinatorial cross-validation

The combinatorial cross-validation is used when the number of data is too poor to have good statistics. First, we define the set of experimental design \mathcal{E} . In this set, we draw randomly [80 %] of them. This new set is defined as $\mathcal{E}_{\text{calib}}$ and the [20 %] remaining are defined as $\mathcal{E}_{\text{valid}}$. Then, the experiments in the set $\mathcal{E}_{\text{calib}}$ will be used to calibrate the model and the experiments in the set $\mathcal{E}_{\text{valid}}$ to validate the model. Thus, the process of calibrating and validating the model is repeated many times. This will allow to test the **predictive power** of the model.

In order to test the **robustness** of the model, a full-set calibration is initially done. The initial vector \mathbf{z}_0 is chosen randomly between the lower and upper bounds. Then, the results of the full-set calibration \mathbf{z}_{FS} is given as initial parameters for the combinatorial cross-validation.

The results presented in section 5 are done with:

- 624 runs of SA² with 161 iterations for the full-set calibration
- 200 runs of SA² with 200 iterations for the combinatorial cross-validation

¹We give here a warning. Using weights for the objective function can bias the results.

²SA stands for Simulated Annealing

4 Data

4.1 HKU – Counter-flow experiments

The first set of data is provided by [Wong et al. \(2010\)](#). In their paper, they present 89 bi-directional experiments varying the total number of pedestrians, the ratio between the two groups and the intersection angle. The reference group is called major group and the conflicting one minor group. They are called like this because the major group consists of at least as many pedestrians as the minor group. We did not get the tracking data, therefore we had to extract manually the travel times of the two groups. Fig 5 shows different frames of the experiments provided by [Wong et al. \(2010\)](#). As we can see, the angle of the camera makes the extraction of the data complicated. Therefore, we avoided to take the cross-flow experiments.

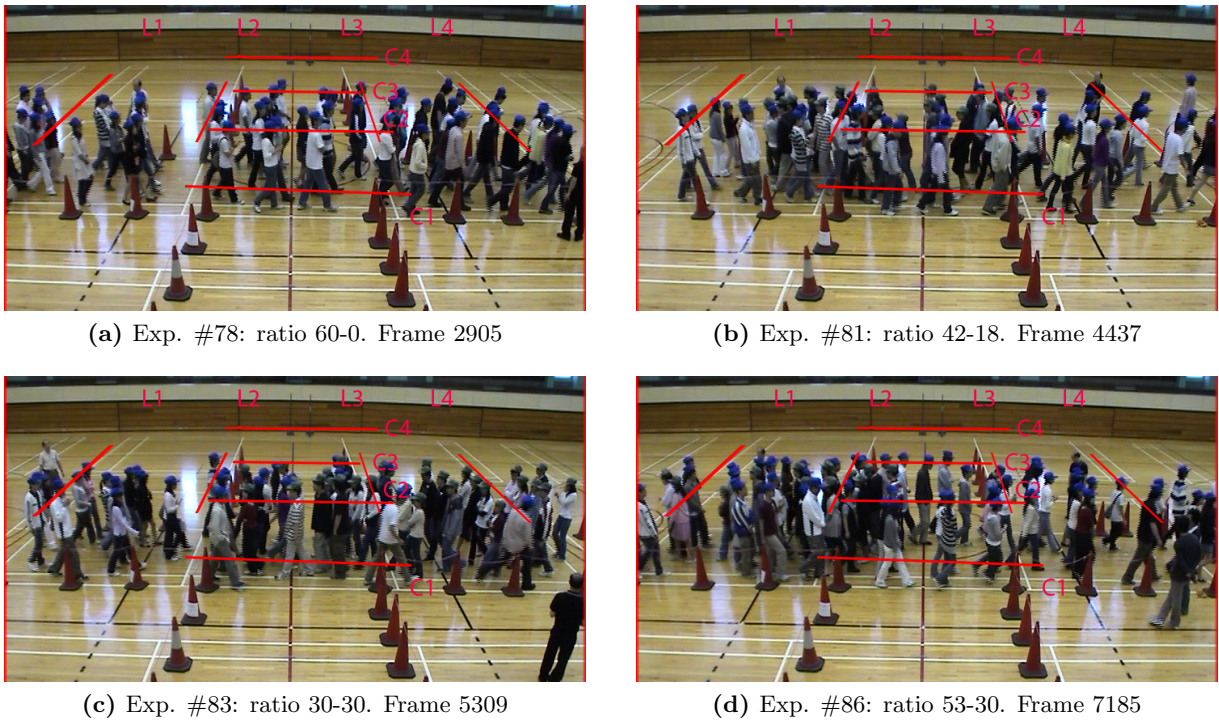


Figure 5: Images of the experimental data provided by [Wong et al. \(2010\)](#). The major group wears blue hats and the minor group wears gray hats.

Fig. 6 shows the walkway configuration for [Wong et al. \(2010\)](#) experiments. The network (a) is the one shown in figure 5. The other setup, (b), was difficult to implement. Thus, we decided to forget it and keep the bi-directional experiments only.

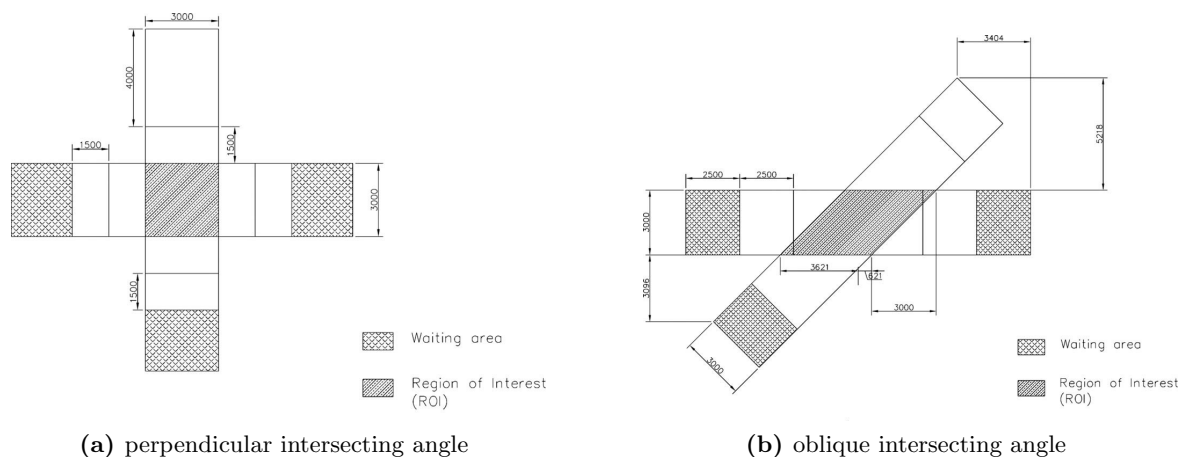


Figure 6: Walkway configuration of the experiment used by Wong et al. (2010).

The bi-directional experiments were done for a total number of pedestrians equal to 40, 60 and 88. Since, we are looking for experiments that show anisotropy, we decided to only take the experiments with a total number of pedestrians equal to 60 and 88. This let us with 12 experiments. The extracted travel times and walking speeds are given in the table 1.

Exp.	# of Ped.		Travel time [s]		Walking speed [m/s]	
78	60	0	10.76	-	0.84	-
79	54	6	10.09	11.26	0.92	0.81
80	48	12	9.27	11.01	0.99	0.83
81	42	18	8.98	11.11	1.02	0.82
82	36	24	9.42	10.28	1.00	0.88
83	30	30	9.78	10.48	0.97	0.87
84	87	0	8.46	-	1.08	-
85	79	9	7.68	11.52	1.19	0.80
86	68	18	10.10	12.66	0.90	0.74
87	61	26	10.98	13.78	0.82	0.67
88	53	30	10.93	11.78	0.83	0.79
89	44	44	11.75	11.61	0.79	0.79

Table 1: Extracted travel times and walking speeds from the chosen experiments by Wong et al. (2010). The major group is in dark gray and the minor group in light gray.

Table 1 shows some anisotropy. Indeed, the travel times and walking speeds are different between the major and the minor groups. In the literature, Lam et al. (2002) has already shown that the walking speed of a minor group walking against a major group is smaller than the walking speed of the major group. It comes from the fact that the speeds (or travel times) are stochastic. Otherwise, for equal counter-flow, we would expect exactly the same speeds, or for higher demands always longer travel times. This means that with more demands, we would always have more congestion. That is not the case in reality.

Fig. 7 illustrates the network used to reproduce the experiments by Wong et al. (2010). The three centered areas (W1, C1, and E1) have a size of 3x3 meters, the gate areas (WGATE, and

EGATE) have an infinite area as the source/sink areas (WEST, and EAST).

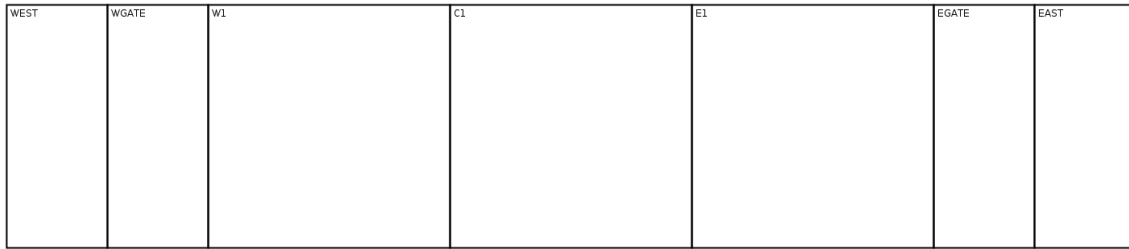


Figure 7: Network used for the model and the experiments provided by Wong et al. (2010). This network is inspired by the walkway (a) in Fig.6. Since only counter-flow experiments are used, the perpendicular walkway is not implemented.

The histograms of the walking speeds for each experiment are presented in the appendix.

4.2 Berlin – “Science Night” experiments

During the *Lange Nacht der Wissenschaften* (Long Night of the Sciences), Plaue et al. (2011) conducted several experiments. A first set of two experiments was under the control of the experimenters. One of these experiments is counter-flow and the other one is cross-flow. A final experiment with less control was conducted with a lot of pedestrians. This was a cross-flow experiment. Fig.8 shows two images of the experiments. The first one, (a), is the cross-flow controlled experiment. The controlled counter-flow experiment is not shown here. The second one, (b), is the ‘uncontrolled’ experiment.



(a) Controlled counter-flow experiment



(b) ‘uncontrolled’ experiment

Figure 8: Images of the experimental data provided by Plaue et al. (2011).

The problem with these data is that the controlled experiments do not show a lot of anisotropy. The number of pedestrians in the major and the minor groups are almost the same. It is not exactly the same, thus we still have some anisotropy and that is why they are still useful. The ‘uncontrolled’ experiment, on the other hand, shows a lot of anisotropy. The extracted travel times and walking speeds are given in table 2.

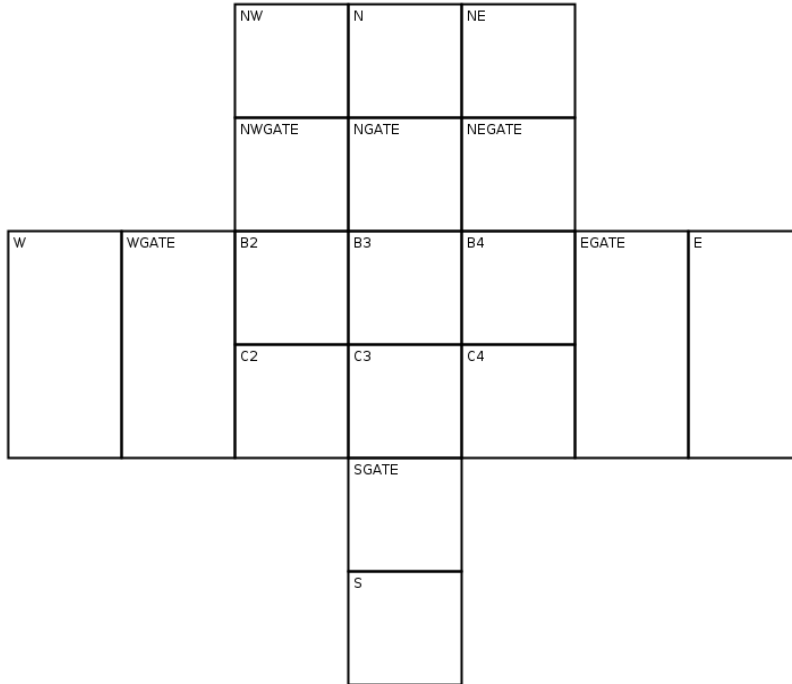
Exp.	# of Ped.		Travel time [s]		Walking speed [m/s]	
Controlled counter-flow	54	46	5.61	5.86	0.98	0.97
Controlled cross-flow	52	46	6.19	4.75	0.91	0.81
‘uncontrolled’cross-flow	134	75	12.30	10.17	0.81	0.59

Table 2: Extracted travel times and walking speeds from the experiments by [Plaue et al. \(2011\)](#). The major group is in dark gray and the minor group in light gray.

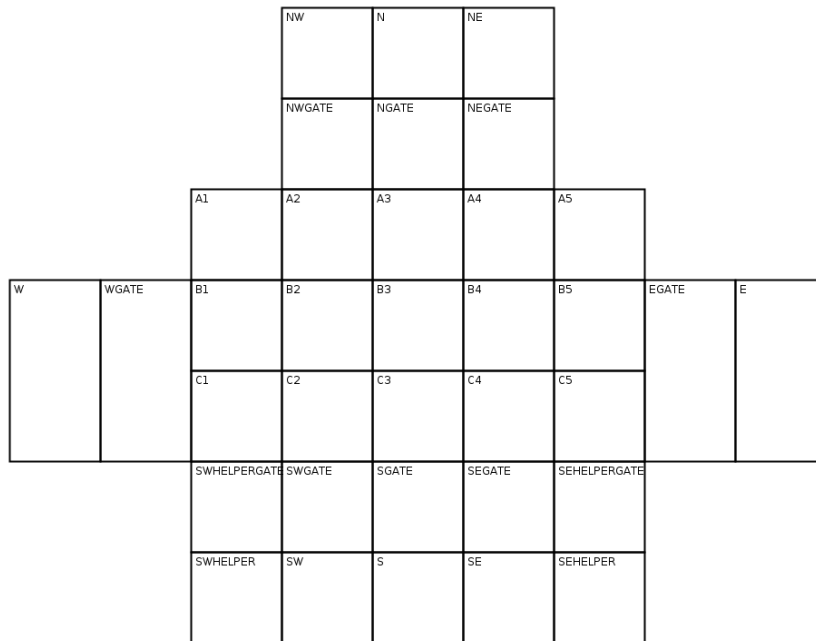
The network is different between the controlled experiments and the ‘uncontrolled’ one. In the ‘uncontrolled’ experiment, pedestrians had a larger choice of routes. Therefore the distance chosen to calculate the walking speed is simply the width and the height of the network for all pedestrians going in the horizontal and vertical directions. The walking speed show that the first two experiments are mostly isotropic because they are almost the same between the two groups. On the other hand, the walking speed of the last experiment shows a larger anisotropy between the major and the minor flow.

[Fig.9](#) illustrates the two networks used to reproduce the experiments by [Plaue et al. \(2011\)](#). All the centered areas (A*, B*, and C*, where * corresponds to a number) have a size of 1.8×1.8 meters. The gate and the source/sinks areas have an infinite area.

The histograms of the walking speeds for each experiment are presented in the appendix.



(a) Network for the controlled experiments



(b) Network for the 'uncontrolled' experiment

Figure 9: Networks used for the model and the experiments provided by [Plaue et al. \(2011\)](#).

5 Results

5.1 HKU – Counter-flow experiments

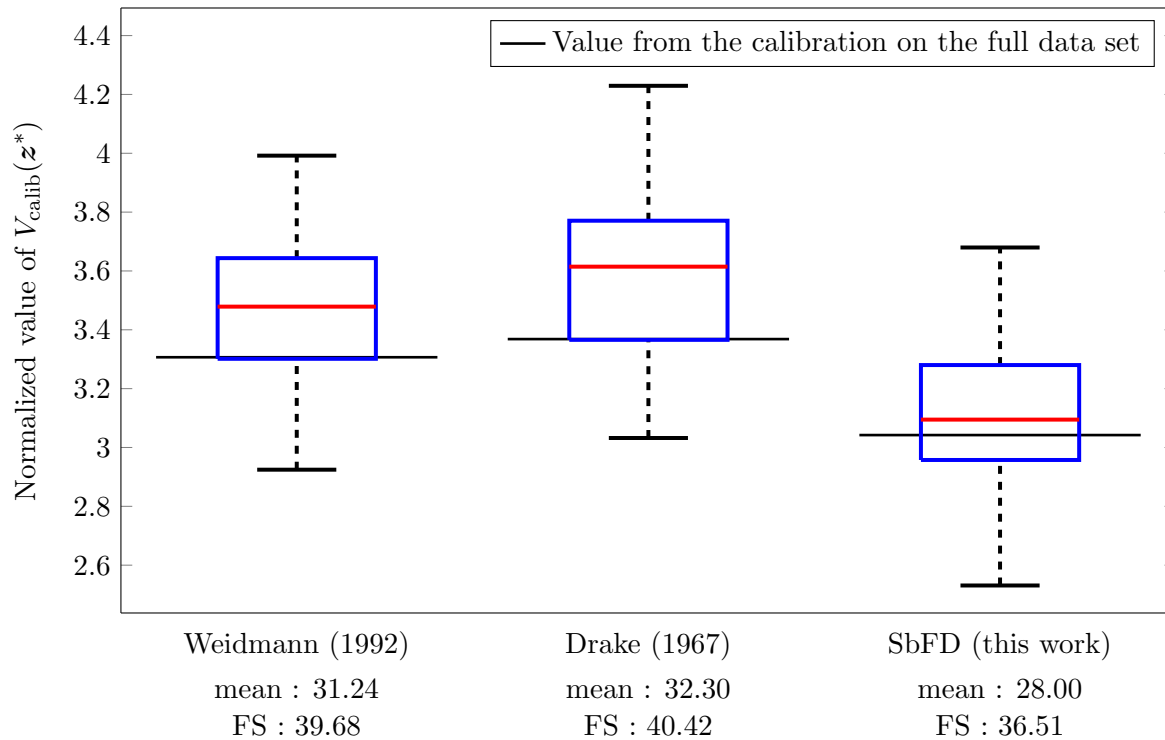


Figure 10: Objective function for each fundamental diagram {Weidmann, Drake, SbFD}. The boxplots are given for the calibration in the combinatorial cross-validation process. The best value from the full-set (FS) calibration is also given with a thin black line. The values on the graph are normalized by the number of experiments, *i.e.* the objective function value for the full-set calibration is divided by 12 and the objective function value for the calibration in the cross-validation process is divided by 9.

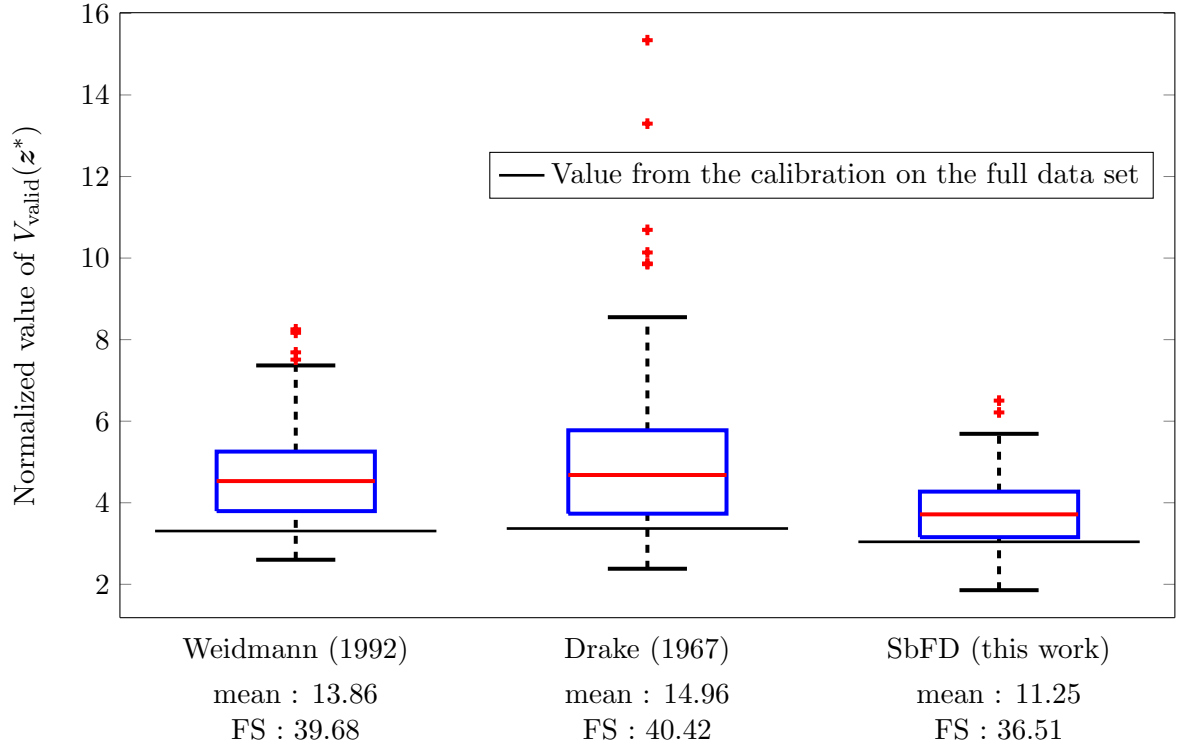


Figure 11: Objective function for each fundamental diagram {Weidmann, Drake, SbFD}. The boxplots are given for the validation in the combinatorial cross-validation process. The best value from the full-set (FS) calibration is also given with a thin black line. The values on the graph are normalized by the number of experiments, *i.e.* the objective function value for the full-set calibration is divided by 12 and the objective function value for the validation in the cross-validation process is divided by 3.

	$V_{\text{calib,FS}}(\mathbf{z}^*)$	$V_{\text{calib,CV}}(\mathbf{z}^*)$	$V_{\text{valid,CV}}(\mathbf{z}^*)$
Weidmann	39.68 (base)	31.24 (base)	13.86 (base)
Drake	40.42 (+1.87%)	32.30 (+3.39%)	14.96 (+7.94%)
SbFD	36.51 (-7.99%)	28.00 (-10.37%)	11.25 (-18.83%)

Table 3: Change in the objective function for the calibration on the full data set ($V_{\text{calib,FS}}(\mathbf{z}^*)$), the calibration in the cross-validation process ($V_{\text{calib,CV}}(\mathbf{z}^*)$) and the validation ($V_{\text{valid,CV}}(\mathbf{z}^*)$). The best value are in green, the worst in red.

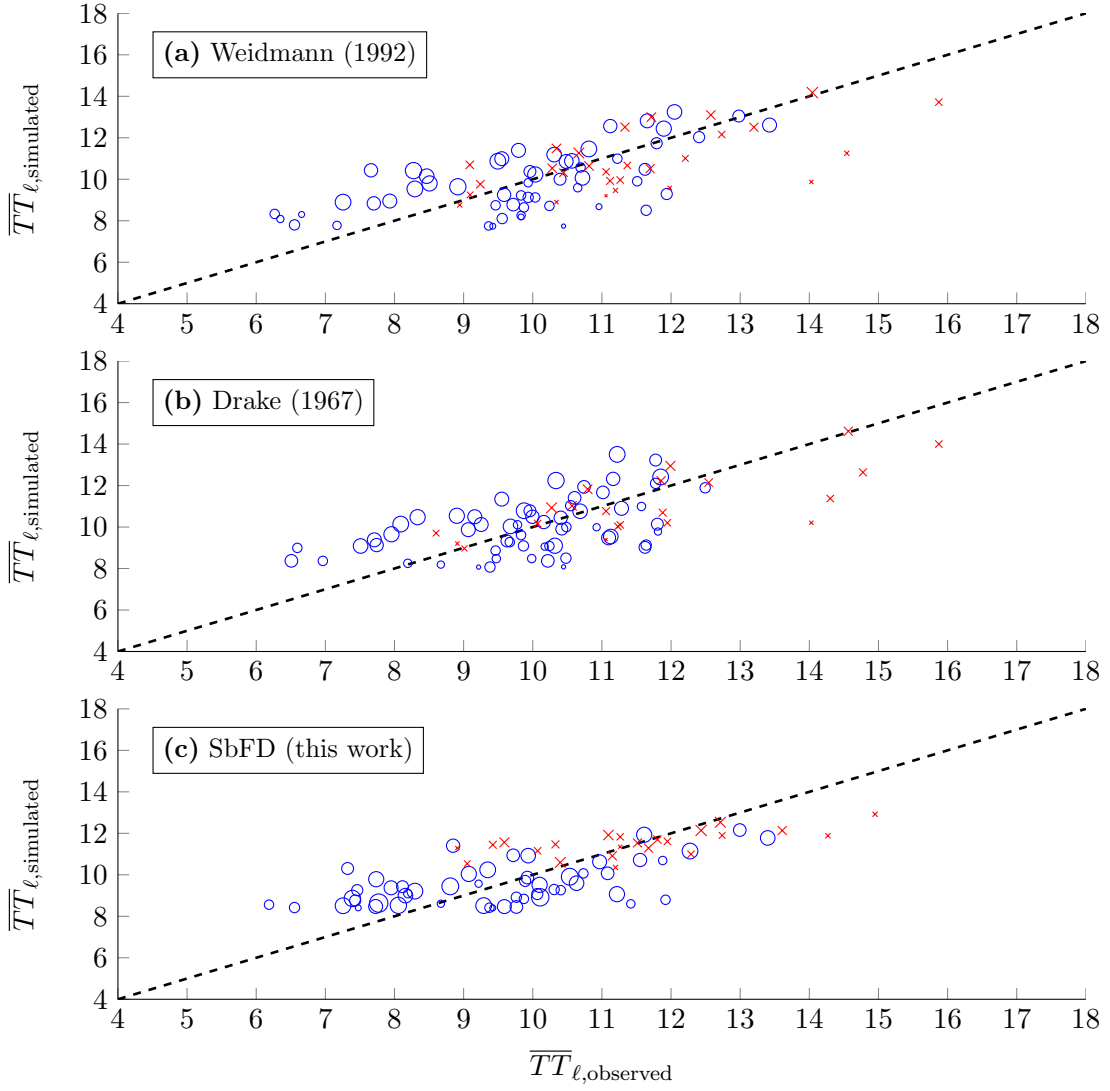


Figure 12: Scatter plot of the run that returns $\min V_{\text{calib}}(\mathbf{z}^*)$, the best run of the combinatorial cross-validation. The blue circles correspond to the major groups and the red crosses correspond to the minor groups. The values associated to these graphs are reported in table 4.

	$\min V_{\text{calib}}(\mathbf{z}^*)$	Run	$\overline{TT}_{\text{Major}}$ [s]			$\overline{TT}_{\text{Minor}}$ [s]			tot
			sim	obs	Δ	sim	obs	Δ	
Weidmann	26.32	180	10.29	9.90	0.39	11.33	11.49	0.16	0.55
Drake	27.29	162	10.28	9.90	0.38	11.48	11.81	0.33	0.71
SbFD	22.78	11	9.60	9.48	0.12	11.57	11.44	0.17	0.29

Table 4: Values extracted from figure 12. \overline{TT} means the weighted average travel time. ‘sim’ and ‘obs’ stand respectively for the simulated and observed travel times. Δ is the absolute value of the difference between the two. ‘tot’ is the sum of the values corresponding to Δ for both the major and minor groups. The red values are the worst and the green the best.

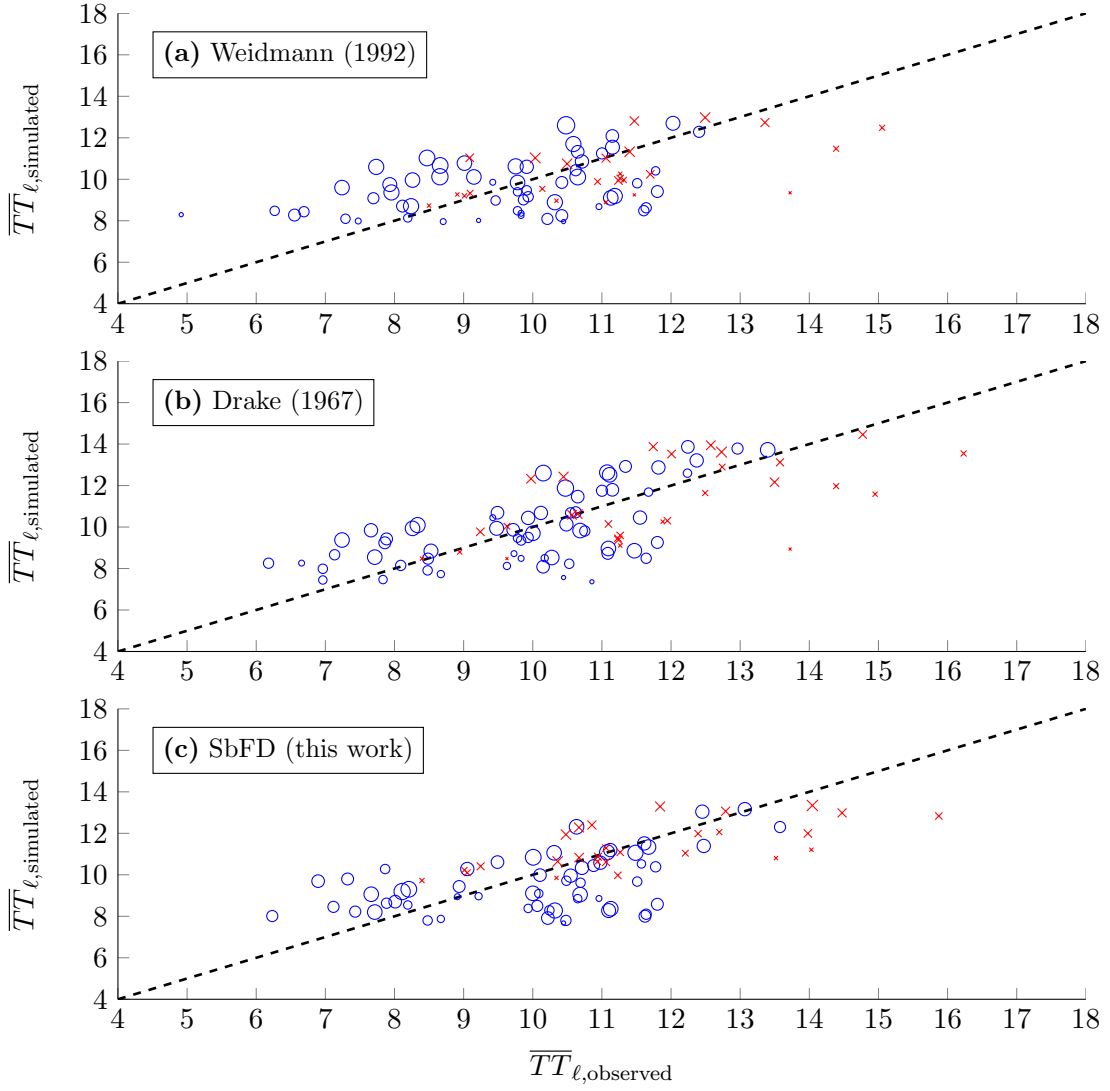


Figure 13: Scatter plot of the run that returns $\max V_{\text{calib}}(z^*)$, the worst run of the combinatorial cross-validation. The blue circles correspond to the major groups and the red crosses correspond to the minor groups. The values associated to these graphs are reported in table 5.

	$\max V_{\text{calib}}(z^*)$	Run	$\overline{TT}_{\text{Major}}$ [s]			$\overline{TT}_{\text{Minor}}$ [s]			tot
			sim	obs	Δ	sim	obs	Δ	
Weidmann	35.93	23	10.01	9.62	0.39	10.97	11.20	0.23	0.62
Drake	39.06	142	10.28	10.03	0.25	11.75	11.80	0.05	0.30
SbFD	33.12	162	9.79	10.07	0.28	11.68	11.67	0.01	0.29

Table 5: Values extracted from figure 13. \overline{TT} means the weighted average travel time. ‘sim’ and ‘obs’ stand respectively for the simulated and observed travel times. Δ is the absolute value of the difference between the two. ‘tot’ is the sum of the values corresponding to Δ for both the major and minor groups. The red values are the worst and the green the best.

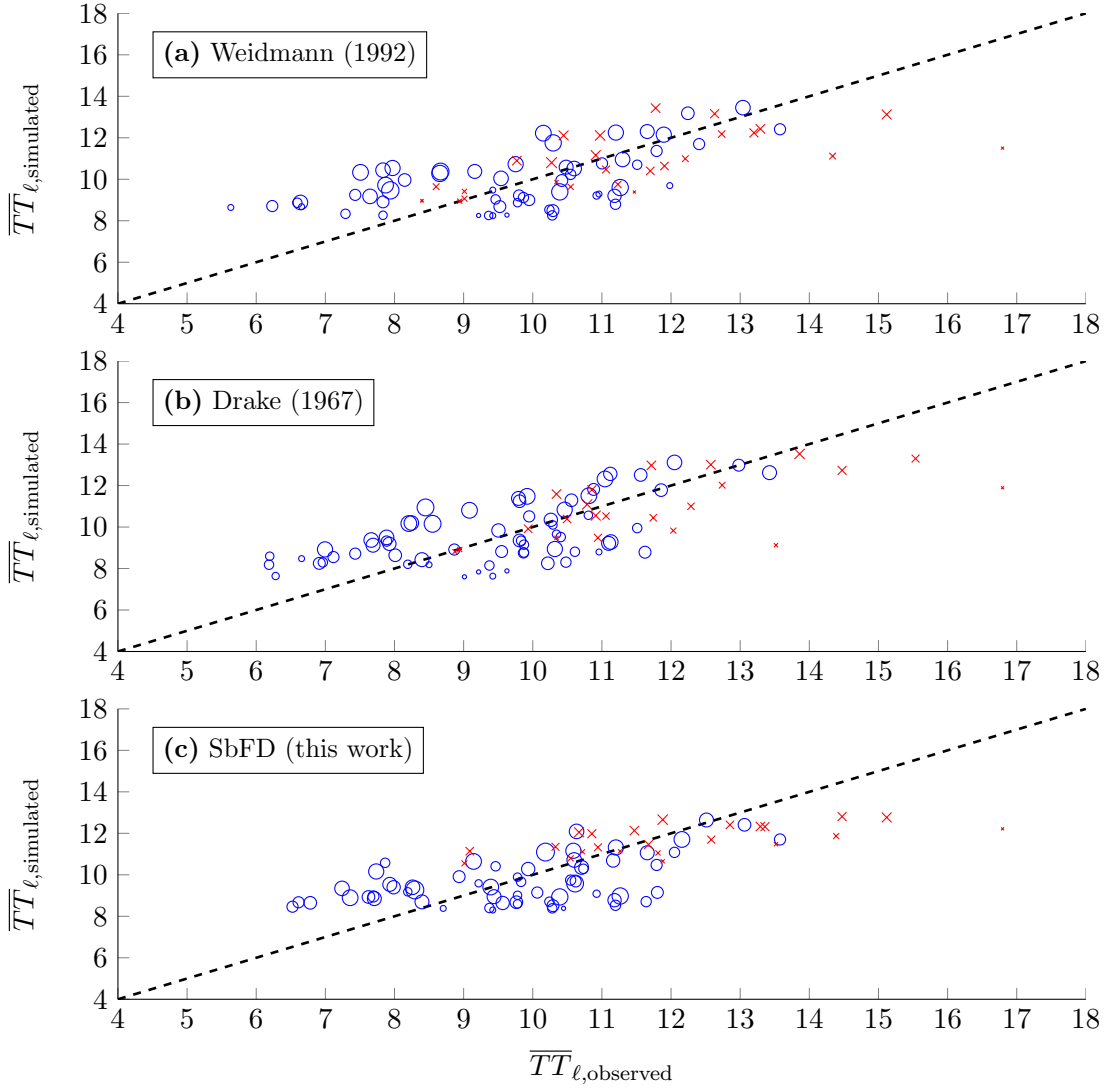


Figure 14: Scatter plot of the run that returns mean $V_{\text{calib}}(z^*)$, the closest run to the average of the combinatorial cross-validation. The blue circles correspond to the major groups and the red crosses correspond to the minor groups. The values associated to these graphs are reported in table 6.

	mean $V_{\text{calib}}(z^*)$	Run	$\overline{TT}_{\text{Major}}$ [s]			$\overline{TT}_{\text{Minor}}$ [s]			tot
			sim	obs	Δ	sim	obs	Δ	
Weidmann	31.24	62	10.25	9.71	0.54	11.38	11.54	0.16	0.70
Drake	32.30	178	10.06	9.57	0.49	11.41	11.78	0.31	0.80
SbFD	28.00	136	9.82	9.79	0.03	11.93	12.06	0.13	0.16

Table 6: Values extracted from figure 14. \overline{TT} means the weighted average travel time. ‘sim’ and ‘obs’ stand respectively for the simulated and observed travel times. Δ is the absolute value of the difference between the two. ‘tot’ is the sum of the values corresponding to Δ for both the major and minor groups. The red values are the worst and the green the best.

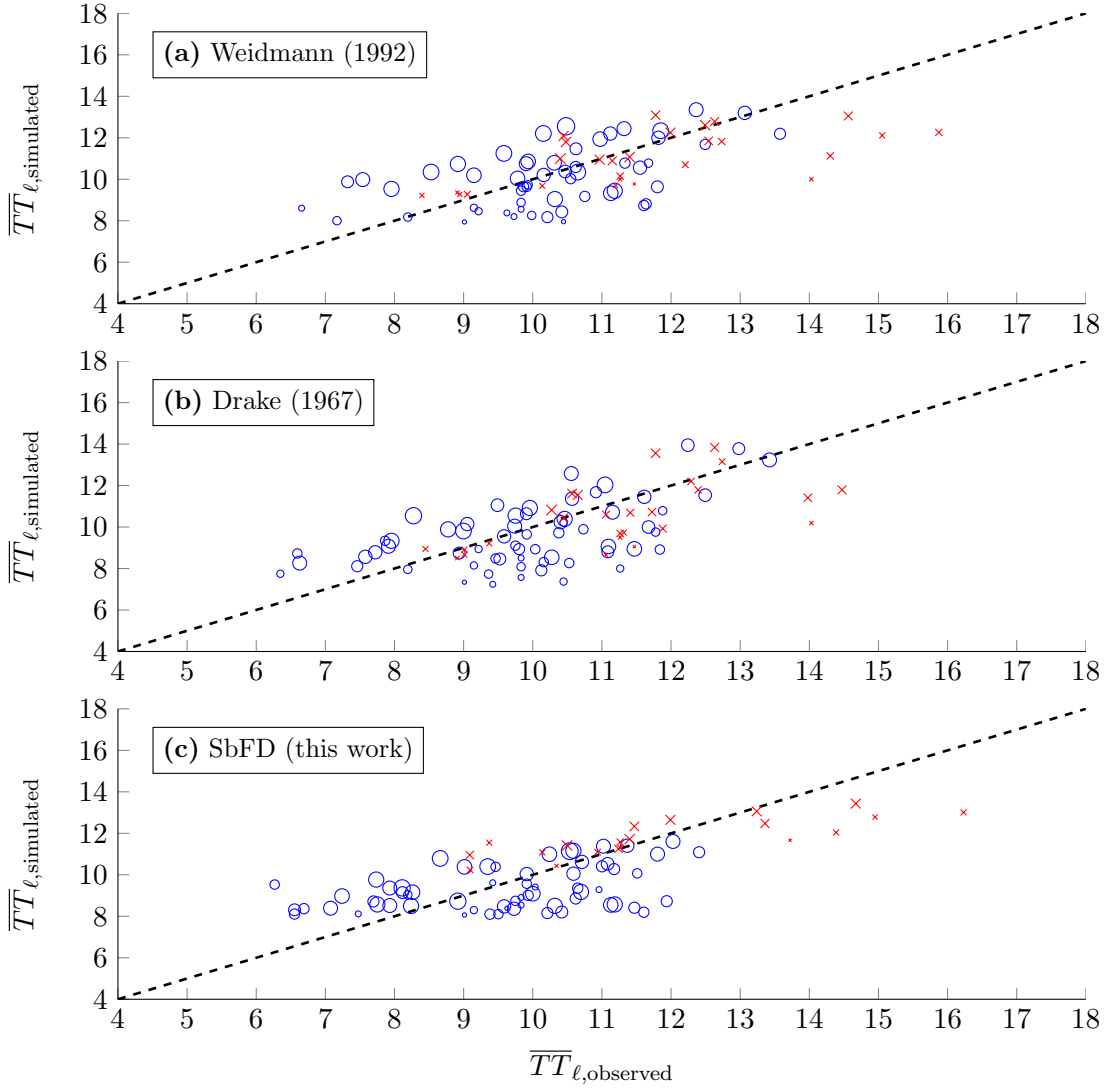


Figure 15: Scatter plot of the run that returns median $V_{\text{calib}}(z^*)$, the median run of the combinatorial cross-validation. The blue circles correspond to the major groups and the red crosses correspond to the minor groups. The values associated to these graphs are reported in table 7.

	median $V_{\text{calib}}(z^*)$	Run	$\overline{TT}_{\text{Major}}$ [s]			$\overline{TT}_{\text{Minor}}$ [s]			tot
			sim	obs	Δ	sim	obs	Δ	
Weidmann	31.31	63	10.55	10.35	0.20	11.49	11.76	0.27	0.47
Drake	32.53	8	9.94	9.93	0.01	11.08	11.43	0.35	0.36
SbFD	27.85	118	9.49	9.61	0.12	11.98	11.89	0.09	0.21

Table 7: Values extracted from figure 15. \overline{TT} means the weighted average travel time. ‘sim’ and ‘obs’ stand respectively for the simulated and observed travel times. Δ is the absolute value of the difference between the two. ‘tot’ is the sum of the values corresponding to Δ for both the major and minor groups. The red values are the worst and the green the best.

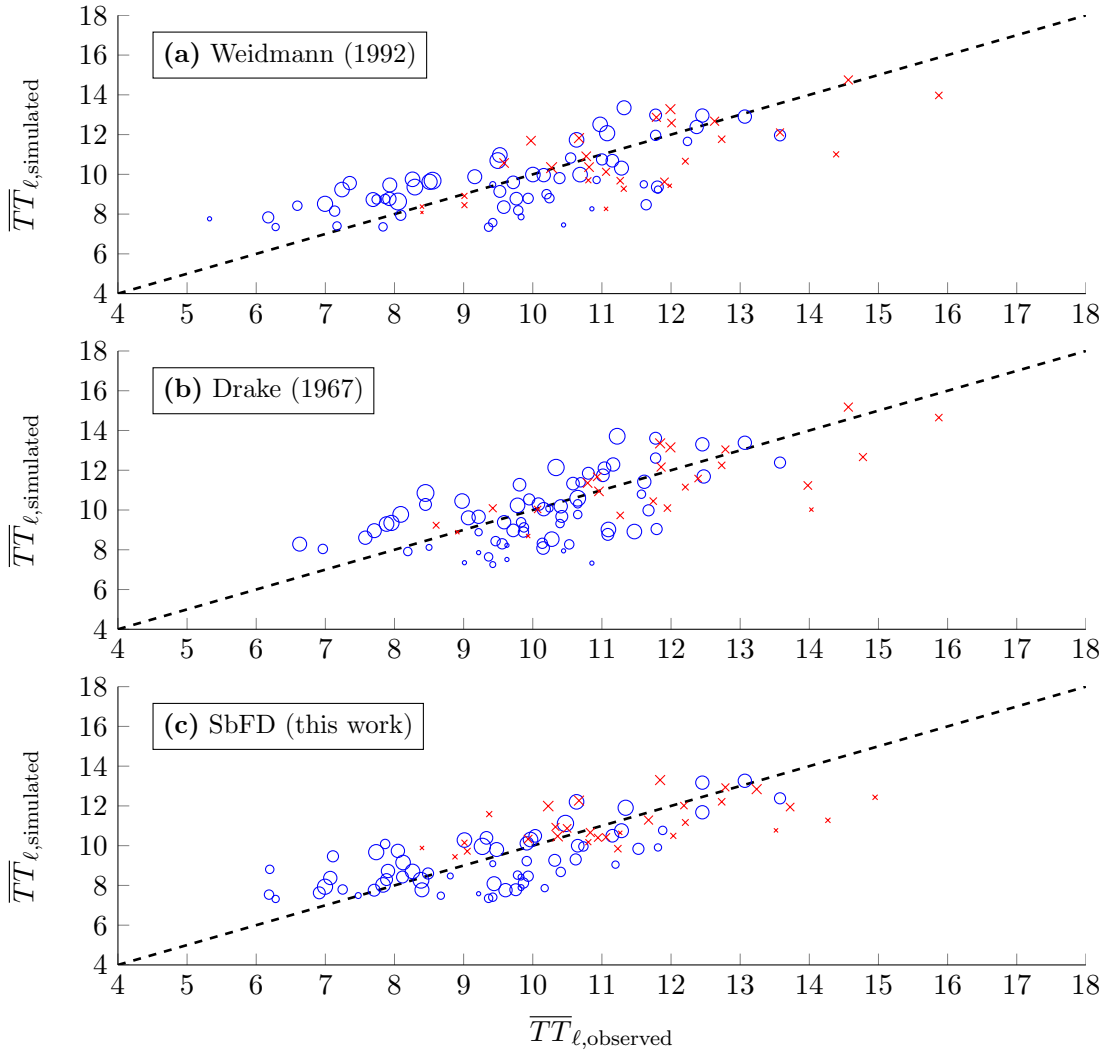


Figure 16: Scatter plot of the calibration run of the combinatorial cross-validation that the linear fit is the closest to the black dashed line: $y = ax + b$, where $a = 1$ and $b = 0$. The fitting of the points has been done with the function `polyfit` from Matlab. The blue circles correspond to the major groups and the red crosses correspond to the minor groups. The values associated to these graphs are reported in the table

	Linear fit		Run	$\overline{TT}_{\text{Major}}$ [s]			$\overline{TT}_{\text{Minor}}$ [s]			tot
	slope	intercept		sim	obs	Δ	sim	obs	Δ	
Weidmann	0.63	3.59	84	9.96	9.62	0.34	11.30	11.53	0.23	0.57
Drake	0.72	2.60	37	10.23	10.06	0.17	11.77	12.01	0.24	0.41
SbFD	0.63	3.47	107	9.49	9.41	0.08	11.34	11.29	0.05	0.13

Table 8: Values extracted from figure 16. \overline{TT} means the weighted average travel time. ‘sim’ and ‘obs’ stand respectively for the simulated and observed travel times. Δ is the absolute value of the difference between the two. ‘tot’ is the sum of the values corresponding to Δ for both the major and minor groups. The red values are the worst and the green the best.

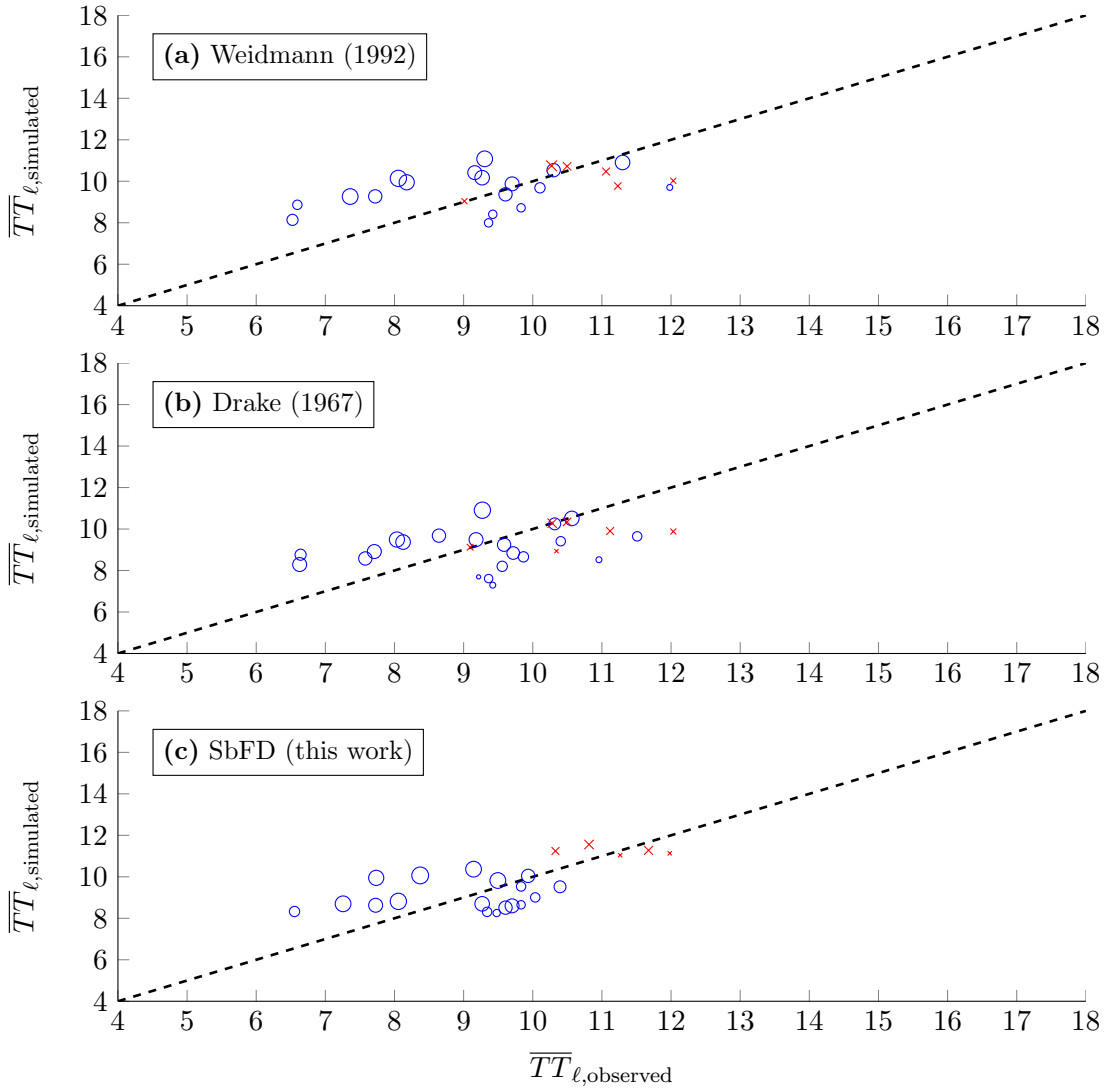


Figure 17: Scatter plot of the run that returns $\min V_{\text{valid}}(\mathbf{z}^*)$, the best run of the combinatorial cross-validation. The blue circles correspond to the major groups and the red crosses correspond to the minor groups. The values associated to these graphs are reported in table 9.

	$\min V_{\text{valid}}(\mathbf{z}^*)$	Run	$\overline{TT}_{\text{Major}}$ [s]			$\overline{TT}_{\text{Minor}}$ [s]			tot
			sim	obs	Δ	sim	obs	Δ	
Weidmann	7.81	51	9.84	8.96	0.88	10.32	10.63	0.31	1.19
Drake	7.15	79	9.32	8.91	0.41	9.94	10.53	0.59	1.00
SbFD	5.57	170	9.24	8.82	0.42	11.34	11.07	0.27	0.69

Table 9: Values extracted from figure 17. \overline{TT} means the weighted average travel time. ‘sim’ and ‘obs’ stand respectively for the simulated and observed travel times. Δ is the absolute value of the difference between the two. ‘tot’ is the sum of the values corresponding to Δ for both the major and minor groups. The red values are the worst and the green the best.

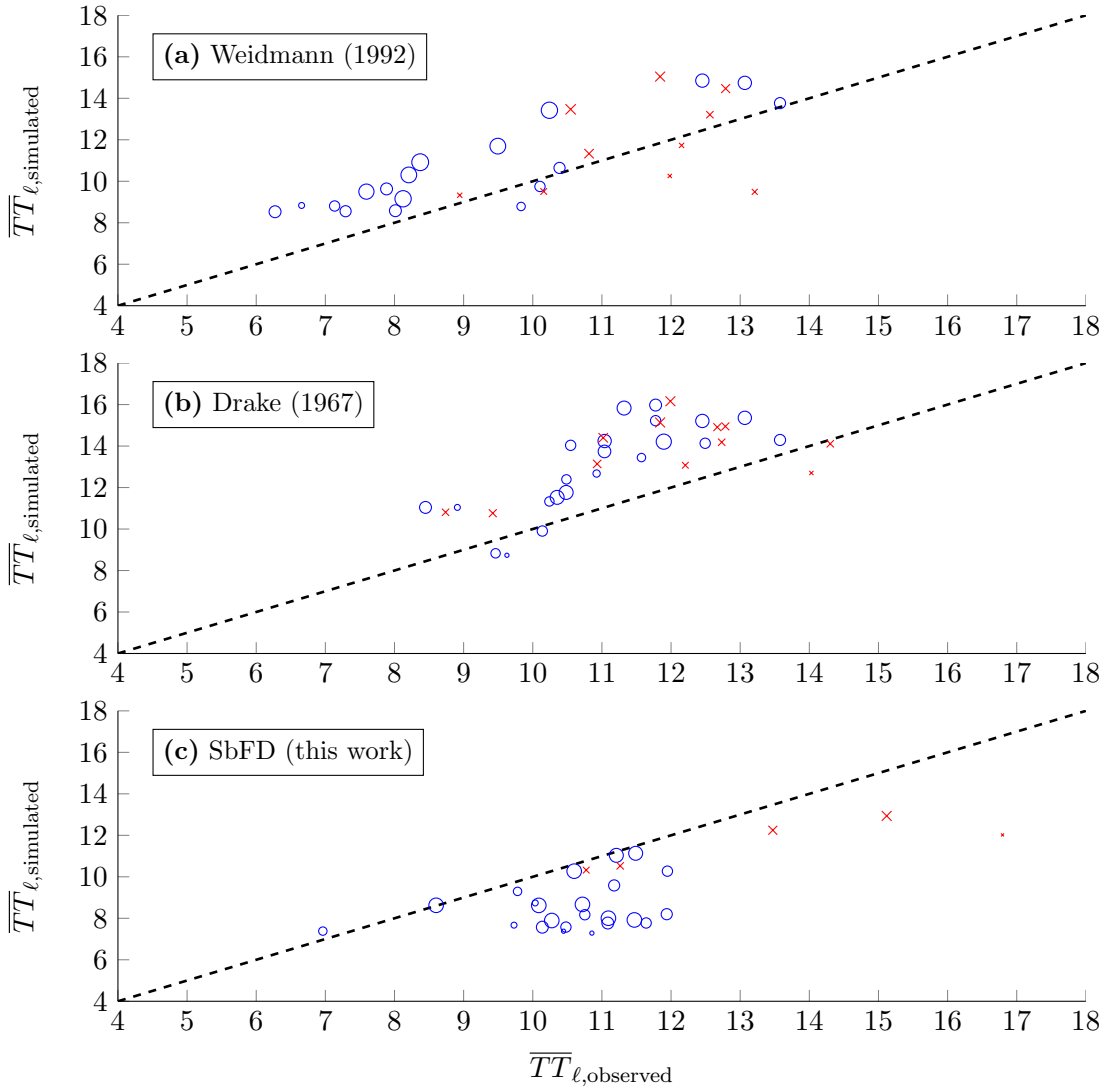


Figure 18: Scatter plot of the run that returns $\max V_{\text{valid}}(z^*)$, the worst run of the combinatorial cross-validation. The blue circles correspond to the major groups and the red crosses correspond to the minor groups. The values associated to these graphs are reported in table 10.

	$\max V_{\text{valid}}(z^*)$	Run	$\overline{TT}_{\text{Major}}$ [s]			$\overline{TT}_{\text{Minor}}$ [s]			tot
			sim	obs	Δ	sim	obs	Δ	
Weidmann	24.76	104	10.88	9.20	1.68	12.60	11.48	1.12	2.80
Drake	46.03	118	13.43	11.19	2.24	14.51	12.22	2.29	4.53
SbFD	19.51	107	8.78	10.64	1.86	11.85	13.31	1.46	3.32

Table 10: Values extracted from figure 18. \overline{TT} means the weighted average travel time. ‘sim’ and ‘obs’ stand respectively for the simulated and observed travel times. Δ is the absolute value of the difference between the two. ‘tot’ is the sum of the values corresponding to Δ for both the major and minor groups. The red values are the worst and the green the best.

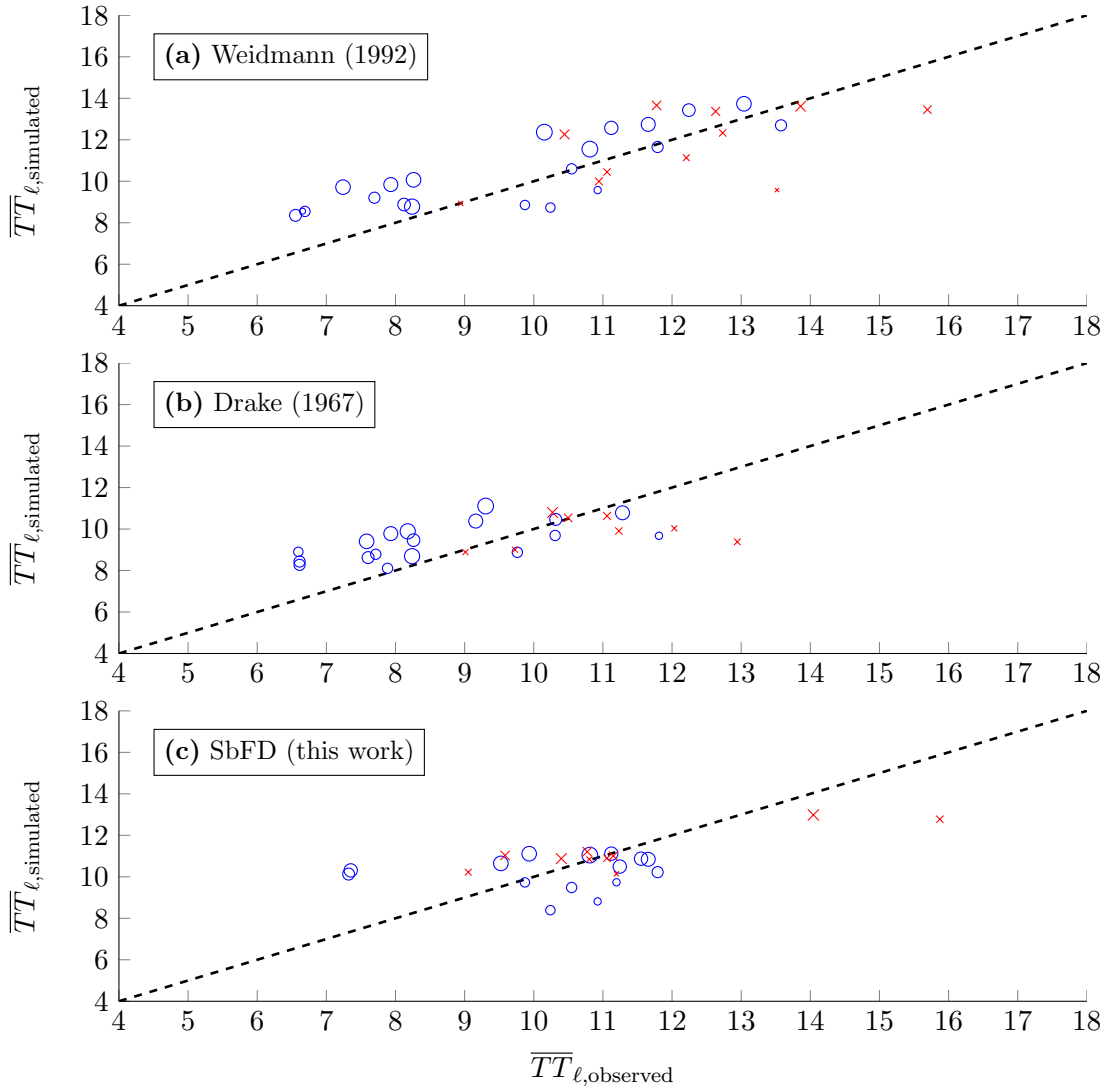


Figure 19: Scatter plot of the run that returns mean $V_{\text{valid}}(\mathbf{z}^*)$, the closest run to the average of the combinatorial cross-validation. The blue circles correspond to the major groups and the red crosses correspond to the minor groups. The values associated to these graphs are reported in table 11.

	mean $V_{\text{valid}}(\mathbf{z}^*)$	Run	$\overline{TT}_{\text{Major}}$ [s]			$\overline{TT}_{\text{Minor}}$ [s]			tot
			sim	obs	Δ	sim	obs	Δ	
Weidmann	13.86	72	10.80	9.77	1.03	12.29	12.31	0.02	1.05
Drake	14.96	186	9.56	8.58	0.98	10.14	10.79	0.65	1.63
SbFD	11.25	171	10.47	10.29	0.18	11.40	11.49	0.09	0.27

Table 11: Values extracted from figure 19. \overline{TT} means the weighted average travel time. ‘sim’ and ‘obs’ stand respectively for the simulated and observed travel times. Δ is the absolute value of the difference between the two. ‘tot’ is the sum of the values corresponding to Δ for both the major and minor groups. The red values are the worst and the green the best.

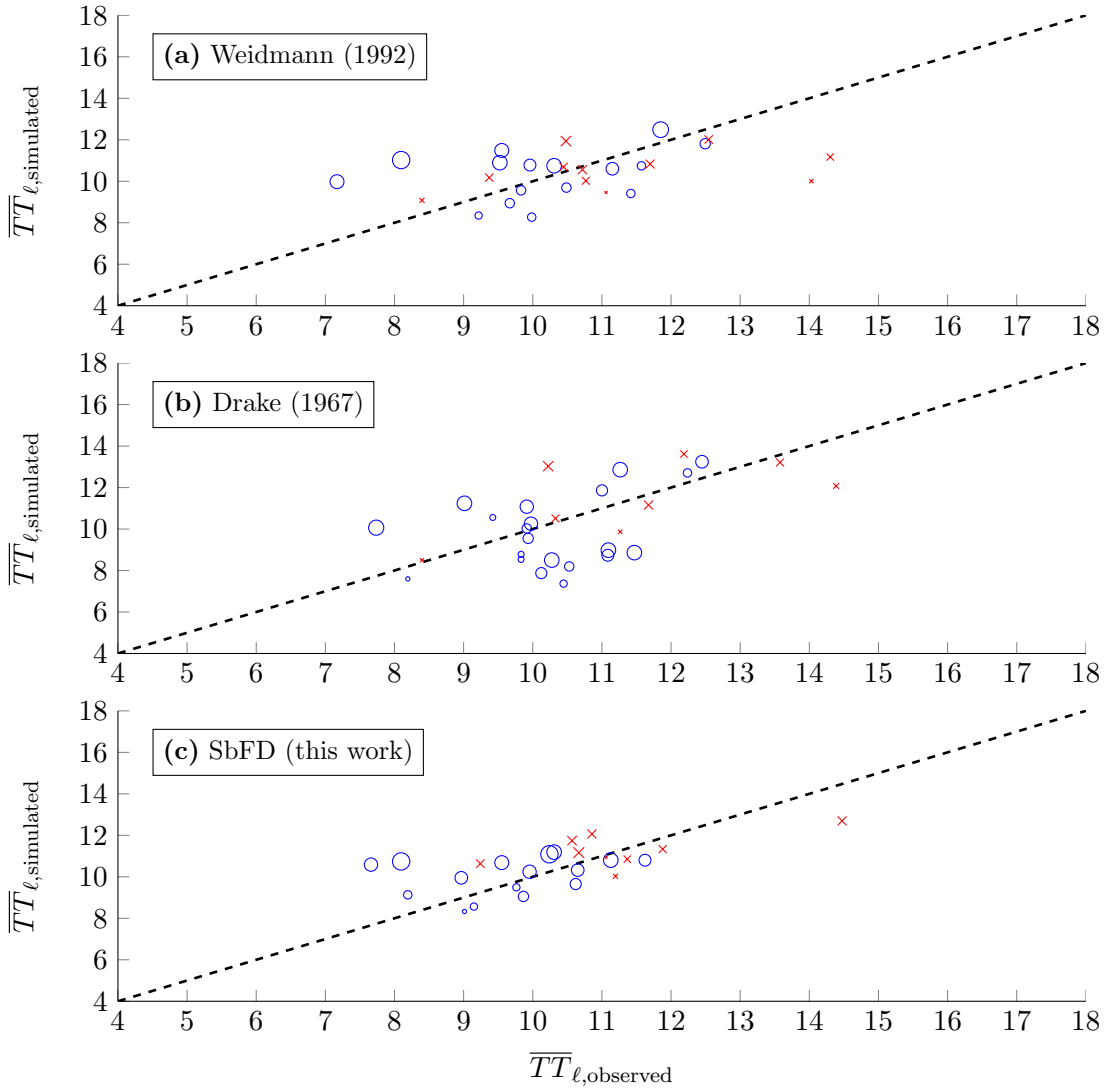


Figure 20: Scatter plot of the run that returns median $V_{\text{valid}}(z^*)$, the median run of the combinatorial cross-validation. The blue circles correspond to the major groups and the red crosses correspond to the minor groups. The values associated to these graphs are reported in table 12.

	median $V_{\text{valid}}(z^*)$	Run	$\overline{TT}_{\text{Major}}$ [s]			$\overline{TT}_{\text{Minor}}$ [s]			tot
			sim	obs	Δ	sim	obs	Δ	
Weidmann	13.59	12	10.70	9.92	0.78	10.86	11.12	0.26	1.04
Drake	14.04	70	10.14	10.35	0.21	12.03	11.53	0.50	0.71
SbFD	11.15	145	10.44	9.73	0.71	11.46	11.25	0.21	0.21

Table 12: Values extracted from figure 20. \overline{TT} means the weighted average travel time. ‘sim’ and ‘obs’ stand respectively for the simulated and observed travel times. Δ is the absolute value of the difference between the two. ‘tot’ is the sum of the values corresponding to Δ for both the major and minor groups. The red values are the worst and the green the best.

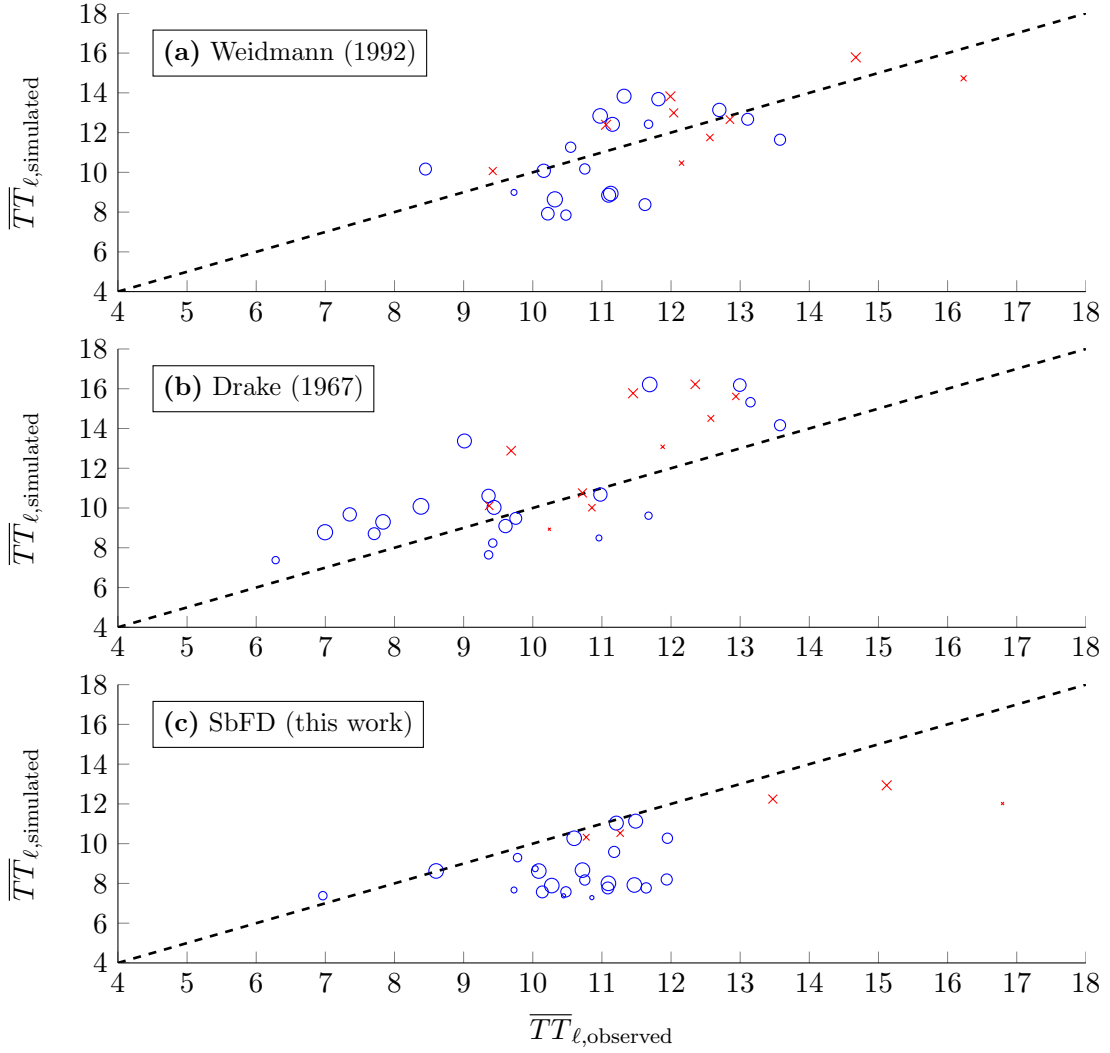


Figure 21: Scatter plot of the validation run of the combinatorial cross-validation that the linear fit is the closest to the black dashed line: $y = ax + b$, where $a = 1$ and $b = 0$. The fitting of the points has been done with the function `polyfit` from Matlab. The blue circles correspond to the major groups and the red crosses correspond to the minor groups. The values associated to these graphs are reported in the table 13.

	Linear fit		Run	$\overline{TT}_{\text{Major}}$ [s]			$\overline{TT}_{\text{Minor}}$ [s]			tot
	slope	intercept		sim	obs	Δ	sim	obs	Δ	
Weidmann	0.91	0.88	45	10.82	11.13	0.31	13.02	12.41	0.61	0.92
Drake	1.11	-0.04	2	10.92	9.56	1.36	13.29	11.14	2.15	3.51
SbFD	0.62	2.19	107	8.78	10.64	1.86	11.85	13.31	1.46	3.32

Table 13: Values extracted from figure 21. \overline{TT} means the weighted average travel time. ‘sim’ and ‘obs’ stand respectively for the simulated and observed travel times. Δ is the absolute value of the difference between the two. ‘tot’ is the sum of the values corresponding to Δ for both the major and minor groups. The red values are the worst and the green the best.

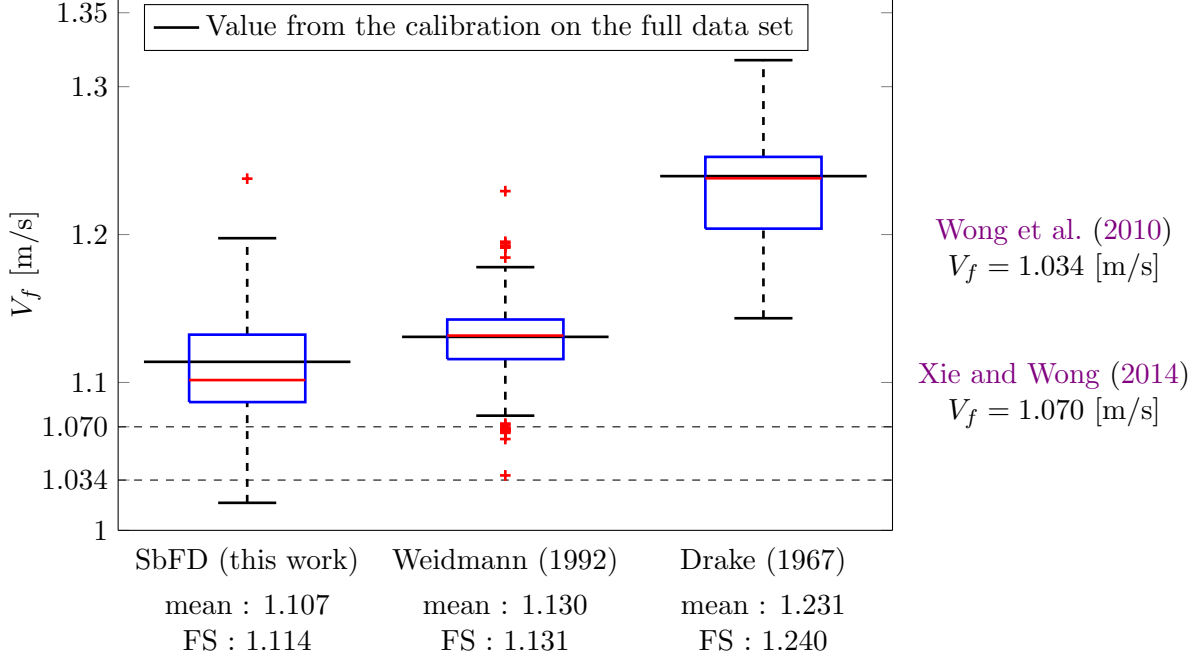


Figure 22: Parameter V_f given for each fundamental diagram. The boxplots represent the values from the calibration in the cross-validation process. The thin black line represents the value returned by the calibration on the full data set. On the left, the values found by Wong et al. (2010) and Xie and Wong (2014) are given.

The figures with the other parameters are presented in the appendix.

5.2 Berlin – “Science Night” controlled experiments

For the results of the controlled experiments, we only show the table of the numerical results. Since there is only two experiments, the cross-validation is done in a different way as it is explain in section 3.3. The idea is to calibrate on one experiment and get the optimal parameters, then we validate on the other experiment with the obtained parameters.

	cross-flow (90°)		counter-flow (180°)	
	calibration	cross-validation	calibration	cross-validation
Weidmann	1.39 (base)	5.63 (base)	0.49 (base)	1.24 (base)
Drake	0.96 (-32.09%)	8.37 (+48.67%)	0.57 (+16.33%)	0.74 (-40.32%)
SbFD	0.93 (-33.09%)	1.63 (-71.05%)	0.47 (-4.08%)	0.71 (-42.74%)

Table 14: Goodness-of-fit for the calibration and the cross-validation for the two controlled experiments. Best values are in green, worst in red.

5.3 Berlin – “Science Night” ‘uncontrolled’ experiment

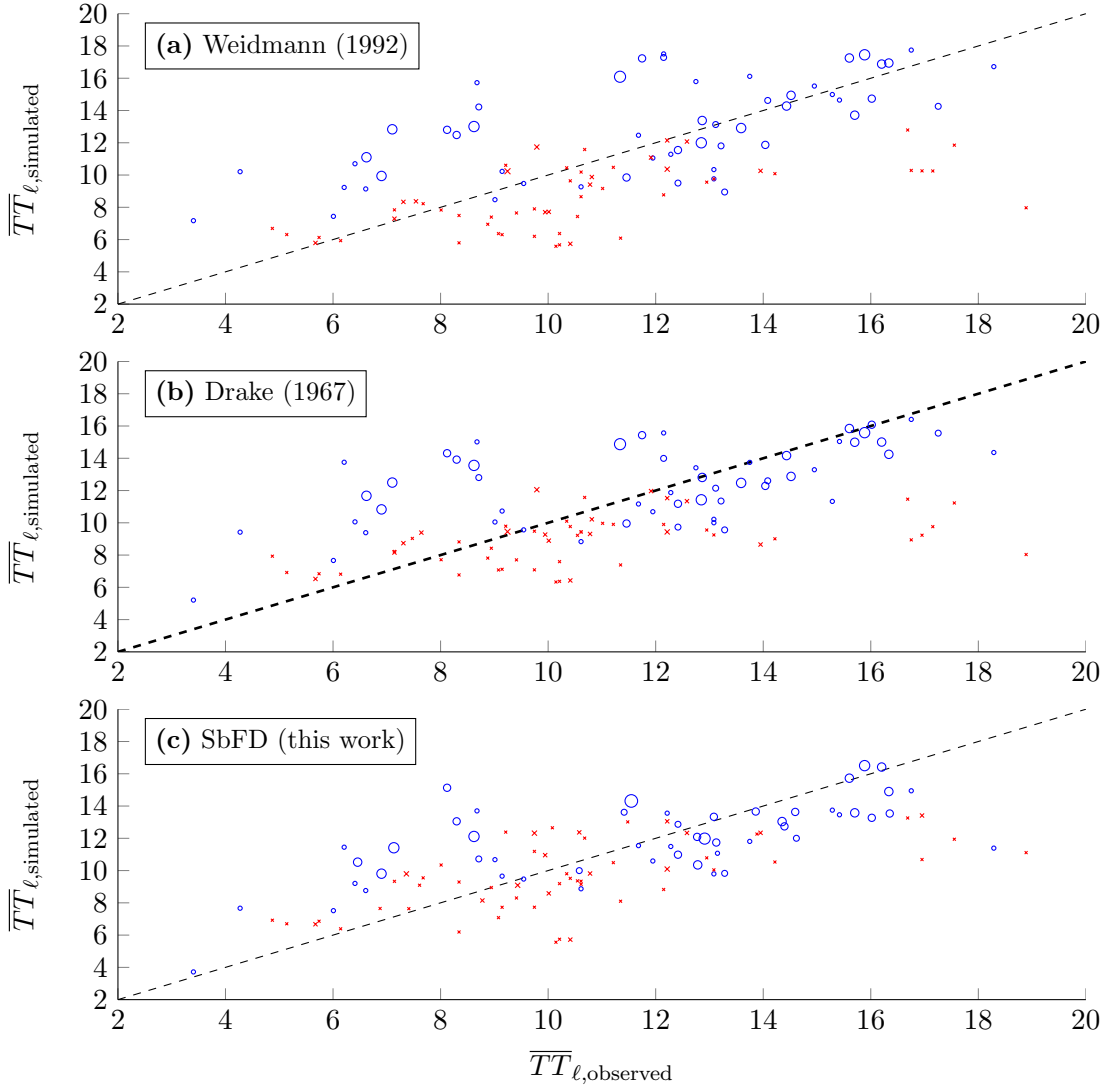


Figure 23: Scatter plot of the run that returns $\min V_{\text{calib}}(\mathbf{z}^*)$, the best run of the combinatorial cross-validation. The blue circles correspond to the major groups and the red crosses correspond to the minor groups. The values associated to these graphs are reported in table 15.

	median $V_{\text{valid}}(\mathbf{z}^*)$	$\overline{TT}_{\text{Major}}$ [s]			$\overline{TT}_{\text{Minor}}$ [s]			tot
		sim	obs	Δ	sim	obs	Δ	
Weidmann	18.02 (base)	13.44	12.04	1.40	8.84	10.44	1.60	3.00
Drake	18.19 (+0.94%)	12.96	12.04	0.92	9.07	10.44	1.37	2.29
SbFD	13.00 (-27.86%)	12.55	12.04	0.51	9.78	10.44	0.66	1.17

Table 15: Values extracted from figure 23. \overline{TT} means the weighted average travel time. ‘sim’ and ‘obs’ stand respectively for the simulated and observed travel times. Δ is the absolute value of the difference between the two. ‘tot’ is the sum of the values corresponding to Δ for both the major and minor groups. The red values are the worst and the green the best.

6 Discussion

The first aspect that comes out of these results is the fact that SbFD performs, most of the time, better than Weidmann and Drake. Indeed, the two figures 10, and 11 and the table 3 show that SbFD is the best fundamental diagram and Drake the worst. We recall here that Drake’s fundamental diagram contains one less parameter than Weidmann and SbFD. The improvement of SbFD on Weidmann, the state-of-the-practice, is between 7.99% and 18.83%. SbFD is the fundamental diagram with the best predictive power. We also see on the two figures that the model is quite robust because the normalized objective function value of the calibration on the full data set stays inside the boxes, *i.e.* 25th and 75th percentiles. This statement is valid mainly for the comparison of the two calibrations.

The different scatter plots show also interesting features. Indeed, if we only compare the objective function, SbFD is the best eight times out of eight. If we compare the difference between the travel times, *i.e.* the value ‘tot’, SbFD performs the best seven times out of ten. Therefore, we can argue that SbFD is not only the fundamental diagram that returns the minimal objective function value, but also the one that returns the least worse value. It is also the one that returns the smallest average and median values most of the time. On the other hand, we see that it really performs less good when we try to fit the reference line. Indeed, on the calibration and on the validation, SbFD is the worst if we only compare the slope and the intercept. This can come from the fact that since it’s an anisotropic fundamental diagram, it will always try to fit the two groups together. It does not take too much into account the whole shape for the two groups together. If a improved specification of such an anisotropic fundamental diagram is developed, then it could maybe take this overall fitting into account.

One last interesting aspect about the parameters found on the calibrations is that they are close to the reality. Indeed, in figure 22, we see that the values of the free-flow speed is close to the values found by Wong et al. (2010) and Xie and Wong (2014). The box plots are overall good, because the overall range for V_f is small. We give, here, just a relative comparison. It is not clear if the difference between the models is significant or not, see last paragraph. We still explain where this difference can come from. We know that the choice of the space discretization can influence the parameter V_f . The experimental data also can. For example, we had a problem with some pedestrians walking too fast.

The Berlin controlled experiments show a small anisotropy in demand, as the extracted data can show, see table 2. This doesn’t stop SbFD to be the best fundamental diagram in all case as the table 14 shows. But, the objective function values between the calibration and the cross-validation are quite different. This is a problem. Indeed, this tells us that the parameter calculated for one of the experiments are not really good for the other experiment. This impairs the robustness of the model between different experiments. On the other hand, we see that this robustness is better with SbFD than the other fundamental diagram.

The Berlin ‘uncontrolled’ experiment has a lot of anisotropy in demand. Therefore, it is logical to see that SbFD performs a lot better than the two other isotropic fundamental diagrams. It suggests that SbFD is a good anisotropic fundamental diagram even if it is not optimal. The discovery of a better fundamental diagram will surely improve the robustness and the predictive power of this model.

All the results presented in the section 5 lack a rigorous statistical testing. The values given in all the tables however show a promising trend in terms of the performance of the proposed model. A rigorous statistical analysis is subject to future research.

are just the one given by the output of the model. Thus, the discussion above is done on results that are not verified correctly. This is why it has to be taken with caution. Indeed, good statistical test would give stronger results and then a better discussion.

7 Conclusion

As the experimental data from Wong et al. (2010), and Plaue et al. (2011) have shown, multi-directional pedestrian flows are generally anisotropic. The new model developed in this project can capture this anisotropy. The use of a simple anisotropic fundamental diagram (SbFD) yields a significant improvement over Weidmann, the state-of-the-practice. Therefore, developing an optimal anisotropic fundamental diagram with different regims and an overall fitting of the travel times may lead to even better results. This will also improve the robustness and the predictive power of this model. As it has been shown, this model is already quite robust and has a good predictive power when the set of experimental data is quite big. One of the problems to calibrate this model was the lack of experimental data showing anisotropy. Only a few of them show an anisotropic behavior. Nevertheless, these few experiments could give enough information to extract the case where the benefit of SbFD is maximal:

- Head-on flow (*e.g.* 180°)
- Asymmetric flow ratio (*e.g.* 10% : 90%)
- High density (*e.g.* $k > 1$ [m⁻²])

This allows us to come back to the illustration of SbFD, see figure 4. On this picture, we already saw that the difference between the speeds of major and minor groups is maximal when it corresponds to the characteristics outlined above.

There is still a lot of work to do in order to well understand pedestrian flows. But this work showed that with a simple anisotropic fundamental diagram and a good model, the prediction of observed travel times can be improved a lot compared to the state-of-the-practice. Of course, this work needs some changes, such as the definition of a better objective function, and the addition of statistical tests on the results. Then, the finding and implementation of an optimal anisotropic fundamental diagram will lead to a significant improvement as compared to the current specification, SbFD.

References

- Hänseler, F. S., Bierlaire, M., Farooq, B. and Mühlematter, T. (2014). A macroscopic loading model for time-varying pedestrian flows in public walking areas, *Transportation Research Part B: Methodological* **69**: 60 – 80.
- Lam, W. H. K., Lee, J. Y. S. and Cheung, C. Y. (2002). A study of the bi-directional pedestrian flow characteristics at Hong Kong signalized crosswalk facilities, *Transportation* **29**(2): 169–192.
- Hänseler, F. S., Lam, W. H. K., Bierlaire, M., Lederrey, G., Nicolici, M. and Scarinci, R. (2015). A dynamic network loading model for anisotropic and congested pedestrian flows. *Memo*.
- Courant, R., Friedrichs, K. and Lewy, H. (1967). On the partial difference equations of mathematical physics, *IBM journal of Research and Development* **11**(2): 215–234.
- Weidmann, U. (1992). *Transporttechnik der Fussgänger*, Schriftenreihe des IVT Nr. 90, Institute for Transport Planning and Systems, ETH Zürich, Switzerland.
- Wong, S. C., Leung, W. L., Chan, S. H., Lam, W. H. K., Yung, N. H. C., Liu, C. Y. and Zhang, P. (2010). Bidirectional pedestrian stream model with oblique intersecting angle, *Journal of Transportation Engineering* **136**(3): 234–242.
- Xie, S. and Wong, S. C. (2014). A Bayesian Inference Approach to the Development of a Multidirectional Pedestrian Stream Model, *Transportmetrica A: Transport Science* (forthcoming): 1–16.
- Drake, J. S. , Schofer, J. L. and May, A. D. (1967). A statistical analysis of speed-density hypotheses, *Highway Research Record* **156** : 53–87.
- Farooq, B., Hänseler, F. S., Mühlematter, T. and Bierlaire, M. (2013). Pedestrian Cell Transmission Model (PedCTM) Calibration, *Memo*.
- Plaue, M., Chen, M., Bärwolff, G. and Schwandt, H. (2011). Trajectory Extraction and Density Analysis of Intersecting Pedestrian Flows from Video Recordings, *Photogrammetric Image Analysis* **6952**: 285–196.

Appendix

Histograms of experiments by Wong et al. (2010) experiments

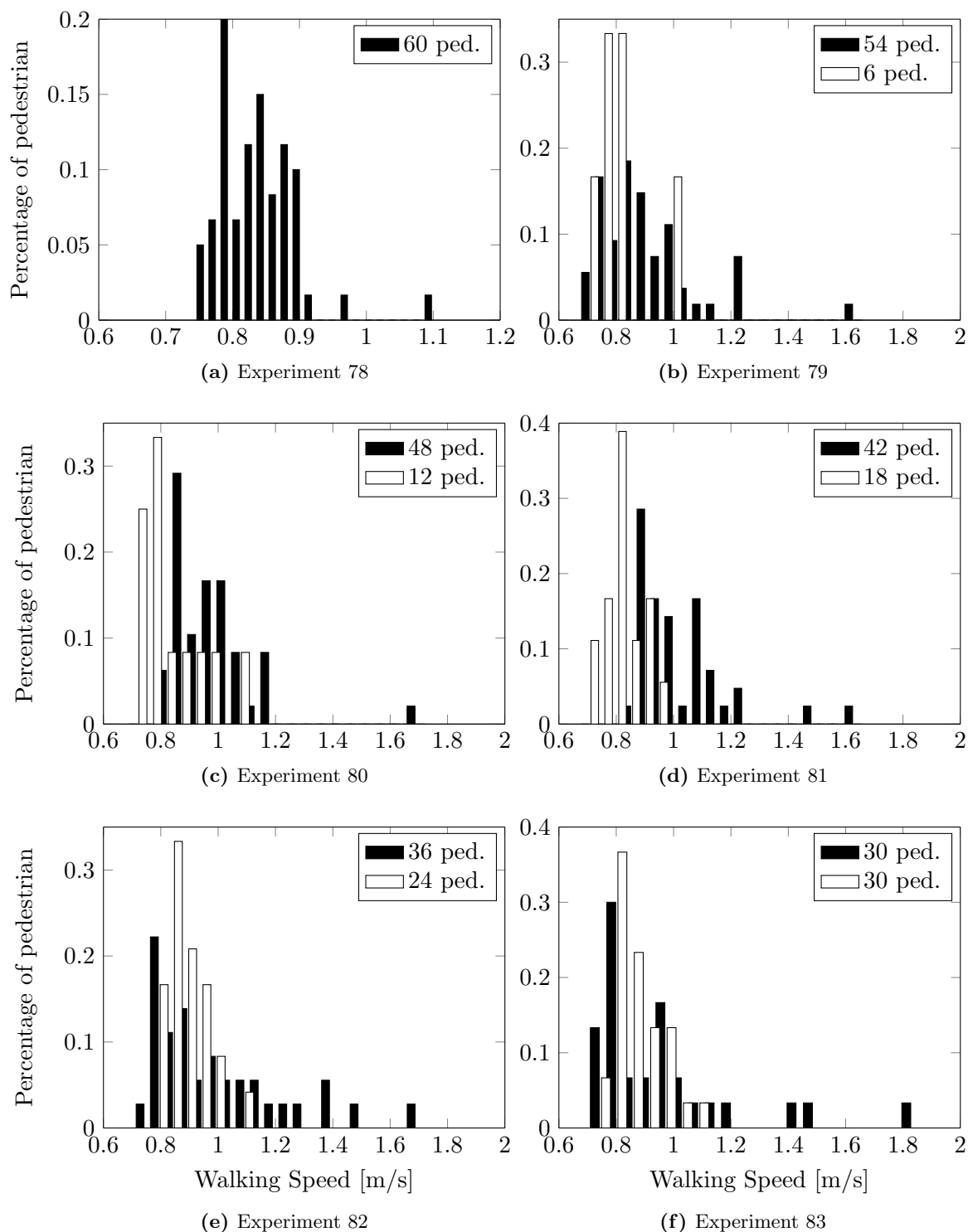


Figure 24: Histograms of the first six experiments by Wong et al. (2010) with a total of approximately 60 pedestrians. The numerical values of the walking speeds are given in the table 1.

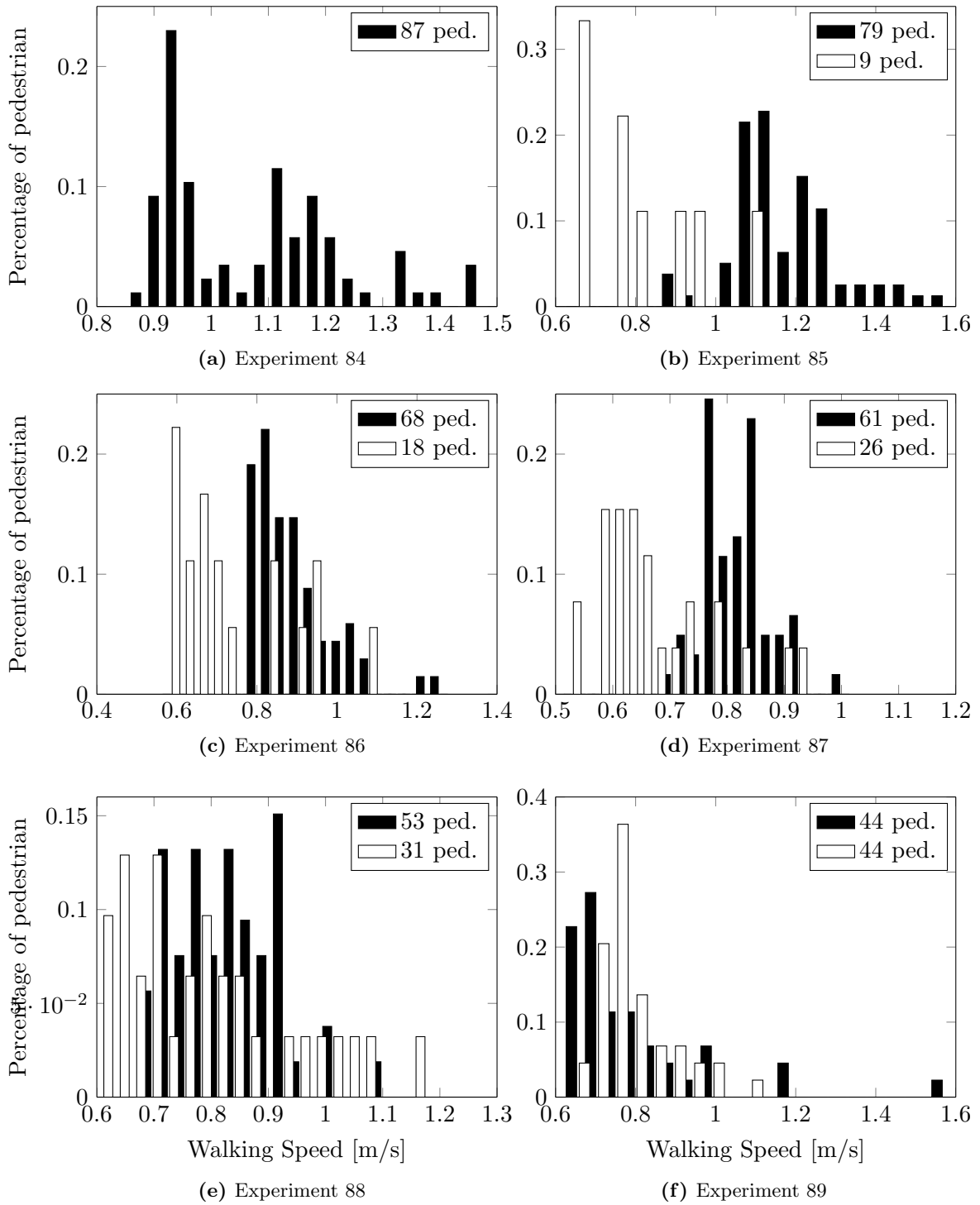


Figure 25: Histograms of the last six experiments by Wong et al. (2010) with a total of approximately 88 pedestrians. The numerical values of the walking speeds are given in the table 1.

Histograms of experiments by [Plaue et al. \(2011\)](#) experiments

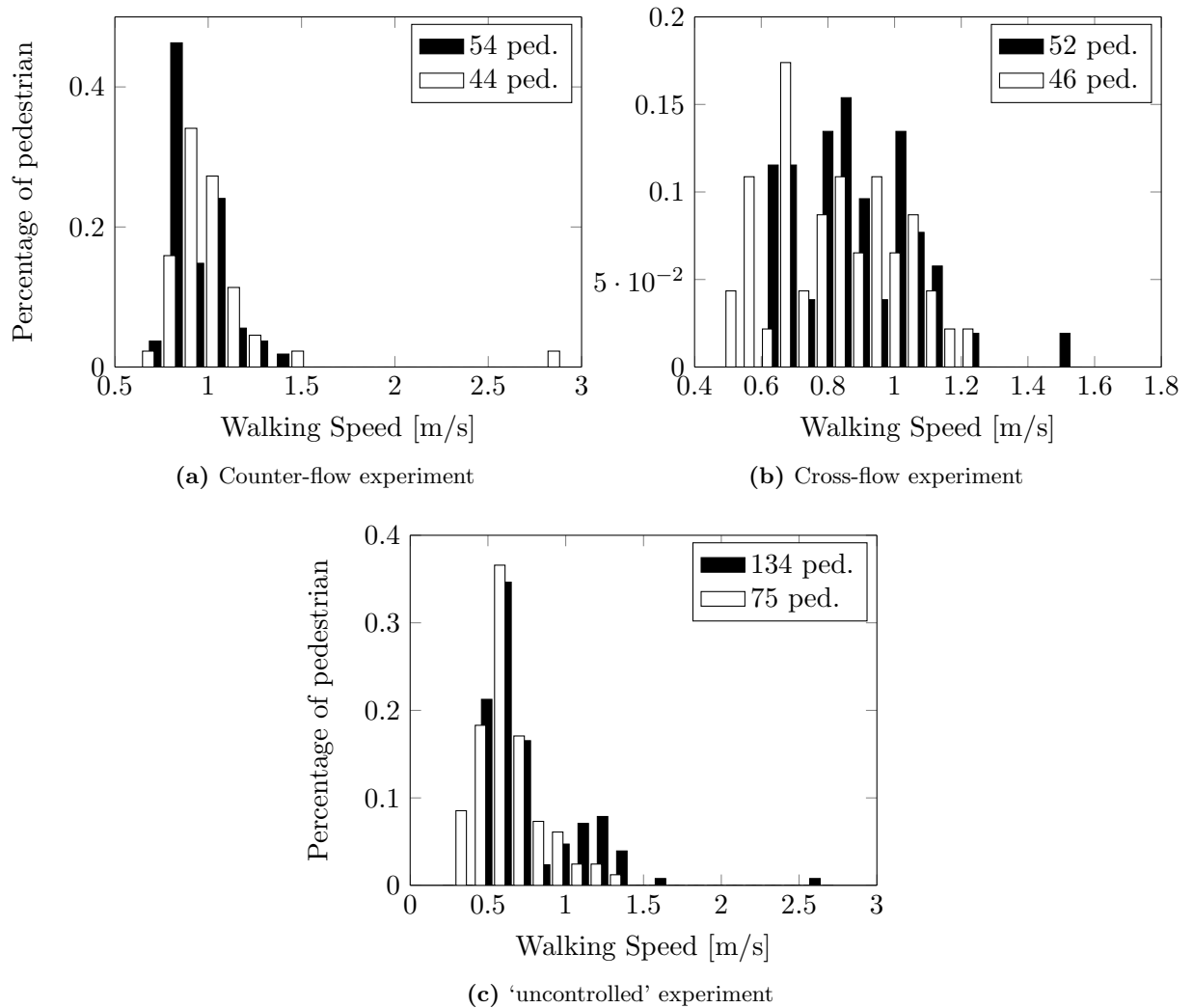


Figure 26: Histograms of the three experiments by [Plaue et al. \(2011\)](#) The numerical values of the walking speeds are given in the table 2.

Boxplots of the parameters

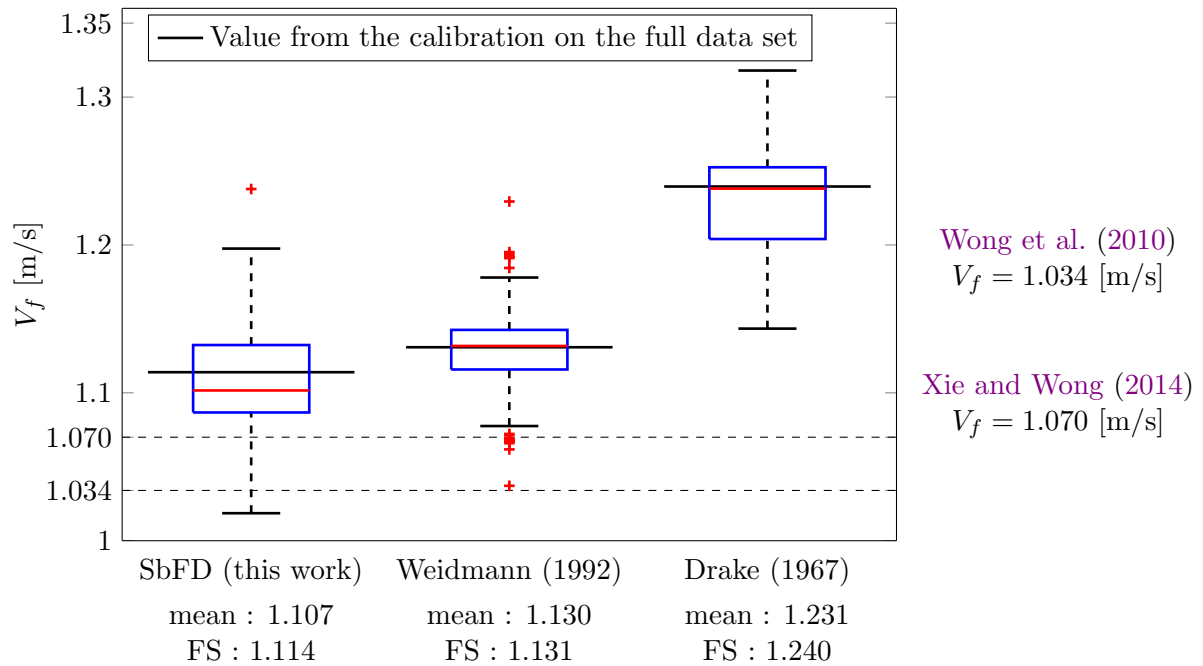


Figure 22: Parameter V_f given for each fundamental diagram. The boxplots represent the values from the calibration in the cross-validation process. The thin black line represents the value returned by the calibration on the full data set. On the left, the values found by Wong et al. (2010) and Xie and Wong (2014) are given.

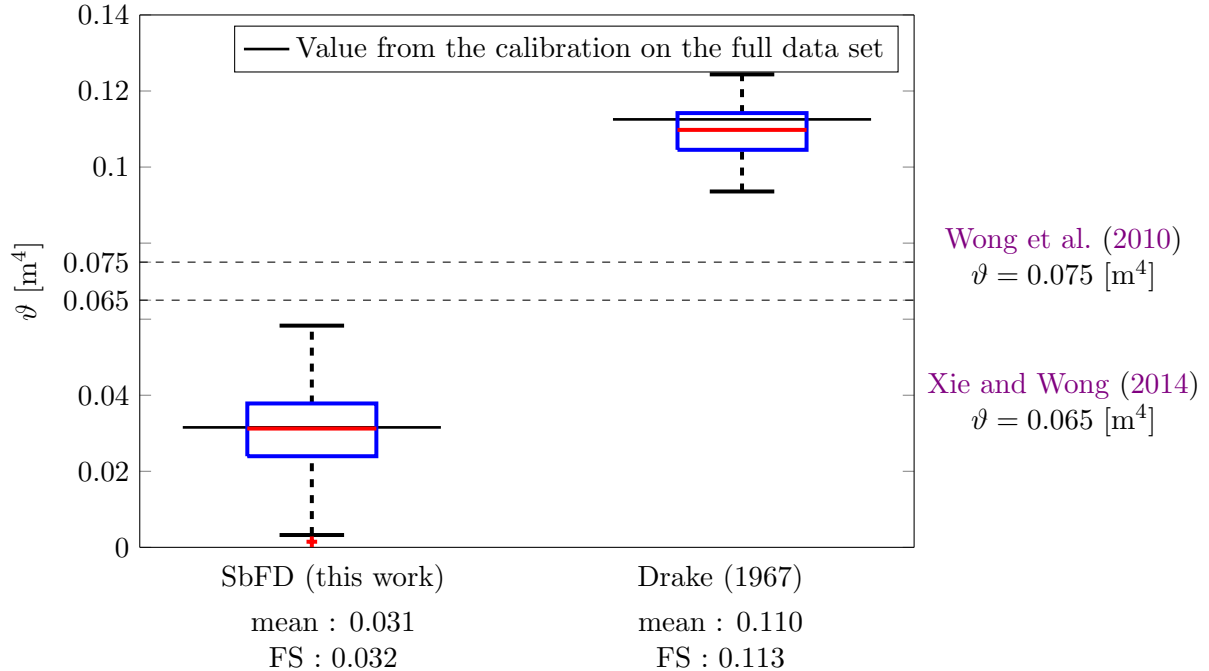


Figure 27: Parameter ϑ given for each fundamental diagram. The boxplots represent the values from the calibration in the cross-validation process. The thin black line represents the value returned by the calibration on the full data set. On the left, the values found by Wong et al. (2010) and Xie and Wong (2014) are given.

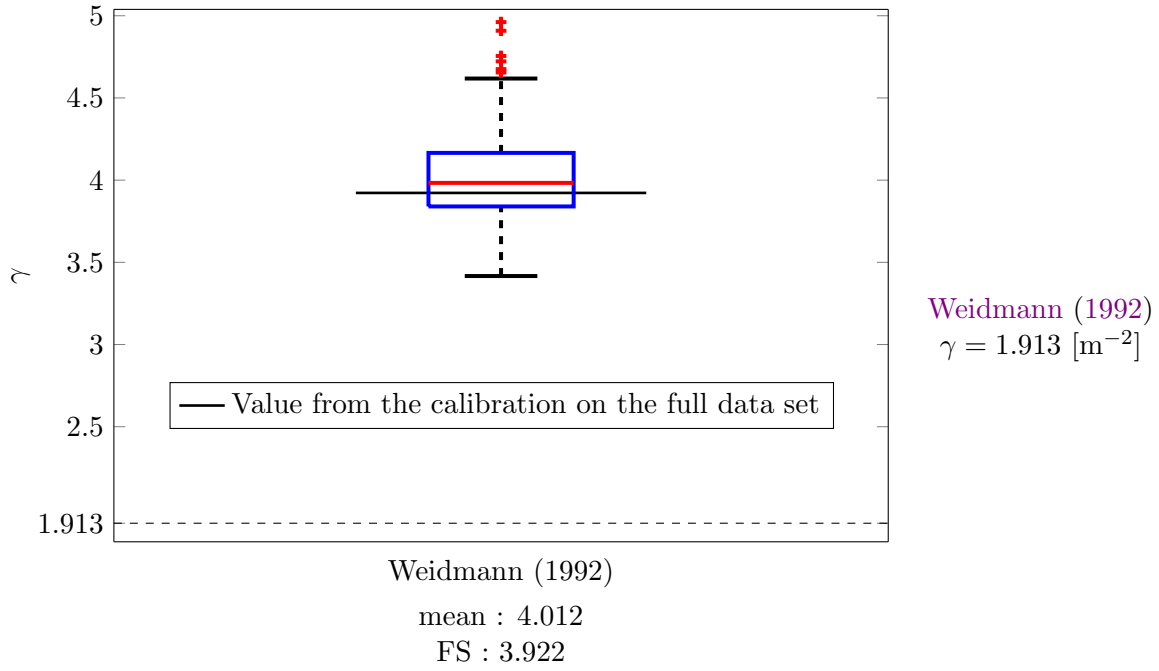


Figure 28: Parameter γ given for Weidmann fundamental diagram. The boxplots represent the values from the calibration in the cross-validation process. The thin black line represents the value returned by the calibration on the full data set. On the left, the value found by Weidmann (1992) is given.

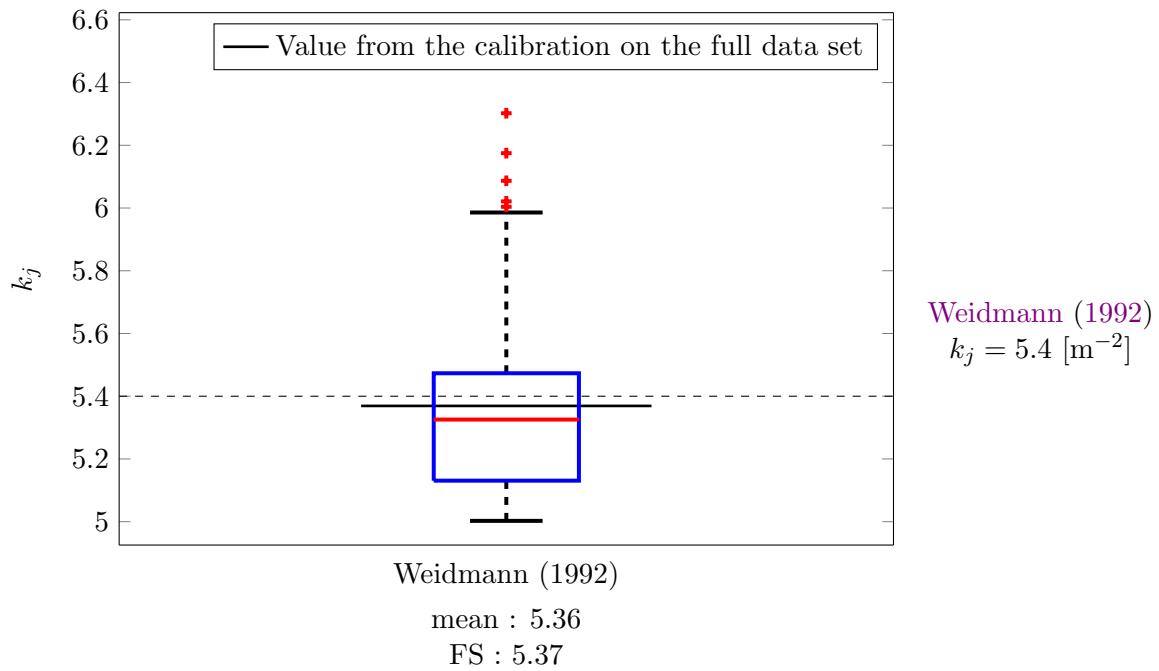


Figure 29: Parameter k_j given for Weidmann fundamental diagram. The boxplots represent the values from the calibration in the cross-validation process. The thin black line represents the value returned by the calibration on the full data set. On the left, the value found by Weidmann (1992) is given.

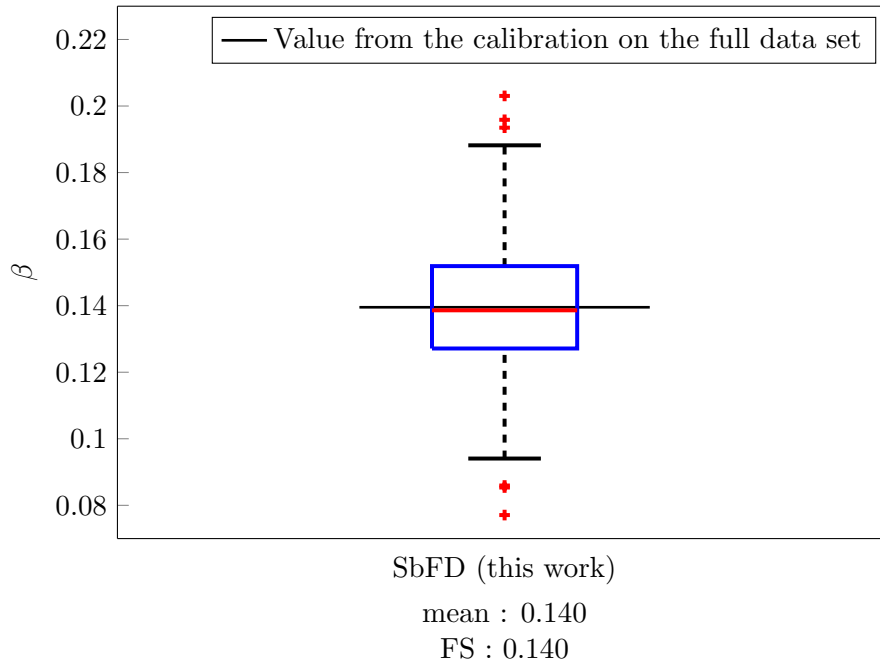


Figure 30: Parameter β given for SbFD. The boxplots represent the values from the calibration in the cross-validation process. The thin black line represents the value returned by the calibration on the full data set. The definition of SbFD changed too much to have a comparison with the β parameter from [Wong et al. \(2010\)](#), and [Xie and Wong \(2014\)](#).

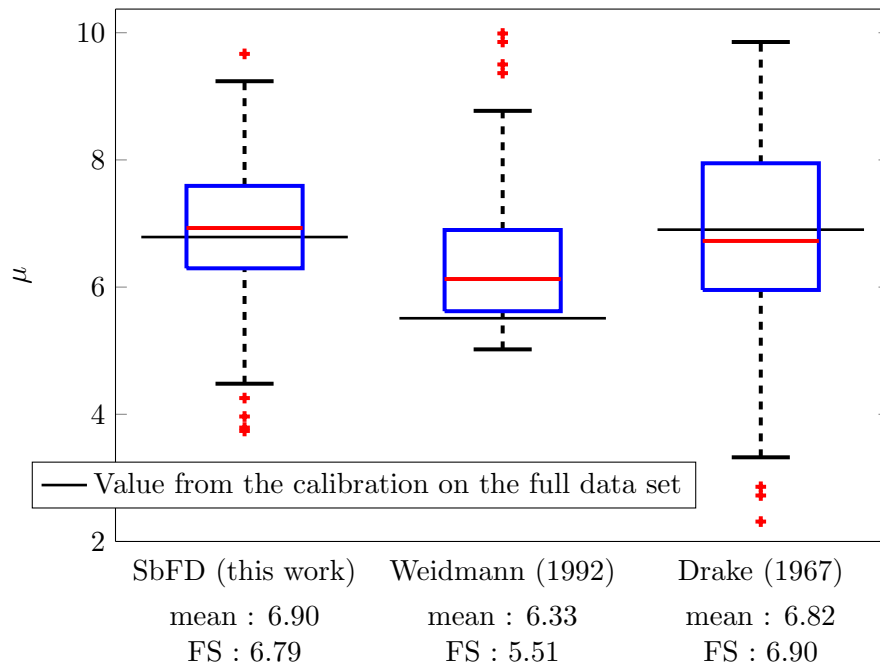


Figure 31: Parameter μ given for each fundamental diagram. The boxplots represent the values from the calibration in the cross-validation process. The thin black line represents the value returned by the calibration on the full data set. There is no comparison with the literature for the parameter μ .